Article

New Petro-Geochemical Data on Carboniferous Mafic Rocks in the Achemmach Area (NW, Fourhal Basin-Moroccan Central Massif)

Hafid Mezougane [1,2,*], Mohamed Aissa [2], Mourad Essalhi [3] , Azizi Moussaid [2], Muhammad Souiri [2], Ahmed Touil [4], Essaid Bilal [5] and Mohamed Souiah [6]

[1] Physico-Chemistry of Processes and Materials Laboratory, Research Team Geology of the Mining and Energetics Resources, Faculty of Sciences and Techniques, Hassan First University of Settat, Settat 26002, Morocco

[2] Department of Geology, Faculty of Sciences, Moulay Ismail University, M.B 11201, Zitoune, Meknes 50070, Morocco; mohamedaissa@gmail.com (M.A.); moussaid.azizi@gmail.com (A.M.); m.souiri@edu.umi.ac.ma (M.S.)

[3] Faculty of Sciences and Techniques, Moulay Ismail University, M.B 509, Boutalamine, Errachidia 52003, Morocco; m.essalhi@umi.ac.ma

[4] Department of Geology, Faculty of Sciences and Techniques, Cadi Ayyad University, M.B 549, Av. AbdelkarimElkhattabi, Gueliz, Marrakech 40000, Morocco; a.touil@uca.ma

[5] Campus of Saint-Etienne 158, National School of Mines of Saint-Etienne (ENSM-SE), Cours Fauriel, 42000 Saint-Etienne, France; bilalessaid@gmail.com

[6] ManagemGroup, Twin Center, Tour A, Angle Boulevards Zerktouni et Al Massira Al Khadra, BP 5199, Casablanca 20250, Morocco; md.souiah64@gmail.com

* Correspondence: hafid.mezougane@uhp.ac.ma

Abstract: The Achemmach region is located 40 km to the SW from Meknes city and 6 km to the NE frm the Hammam mine. It is part of the Paleozoic massif of Central Morocco. The studied area is formed by two Paleozoic rock-types: (i) a meta-sedimentary sequence composed of Middle Visean limestone and shale-sandstone withflyschoid of Upper Visean-Namurian age, and (ii) a magmatic rock series represented by volcanic rocks (pillow-lavas), hypovolcanic rocks (dolerites) and olivine-bearing gabbros.Based on the emplacement model, structural framework, relative chronology and petrogeochemistry of the magmatic rocks, for the first time in this area we distinguish: (i) dm to m-sized greenish pillow-lavas, with sharp borders and radius fractures underlined by fine greenish pelitic sedimentary intercalations, indicating recurrent volcanic activity in short episodes. Plagioclases and pyroxenes (augite) microlites, and more rarely phenocrystals, are recognizable in a glassy matrix devoid of recognizable olivine. (ii) Deformed, metamorphosed and altered dolerites dikes intrude the Middle to Upper Visean shale-sandstone formations. They have an overall NE-SW direction with a NW dip. They are composed of sericitized plagioclases, associated with partially to totally amphibolitized pyroxenes, tourmaline with differentdegrees of chlorite substitution, rutile and opaque minerals, in a microliticmesostasis and (iii) olivine-bearing gabbros, outcropping in variable dimensions (a few meters to 20 m). The olivine-bearing gabbros have a granular texture and are mainly made of plagioclases, pyroxenes, olivine, titanite, rutile, apatite and opaque minerals. All igneous minerals have undergone different degrees of replacement by secondary minerals; plagioclases are sericitized and albitized, pyroxenes are amphibolitized and epidotized and olivine is serpentinized and chloritized. Thepetro-geochemical study of these magmatic bodies demonstrates that pillow-lavas basalts and olivine-bearing gabbros have an alkaline affinity, while dolerites are thought to have a transitional alkaline affinity (alkaline-tholeiitic). Therefore, these formations would have been set up in anorogenic intra-continental geodynamic context, corresponding to a basin magmatism in the little evolved opening.

Keywords: petrogeochemistry; basic magmatic rocks; geodynamic context; NNE Achemmach region; central Morocco

1. Introduction

The NNE sector of Achemmach is situated at 40 km south west of Meknes city and 5 km east of the El Hammam fluorite mine. It is in the north-eastern part of the Hercynian Moroccane Central Massif (HMCM), which constitutes one of the main units of the Mesetian domain corresponding to the main orogenic zone of the Moroccan Variscan belt (Figures 1 and 2). In addition to the heterogeneity of its structural framework, this domain is characterized by the occurrence of a set of magmatic events in a contrasting metamorphic environment. Generally, these are magmatic plutons (granites) or dikes and sills (microgranites and dolerites) or volcanic rocks (basaltic pillow-lavas) intercalated within the sedimentary formations.
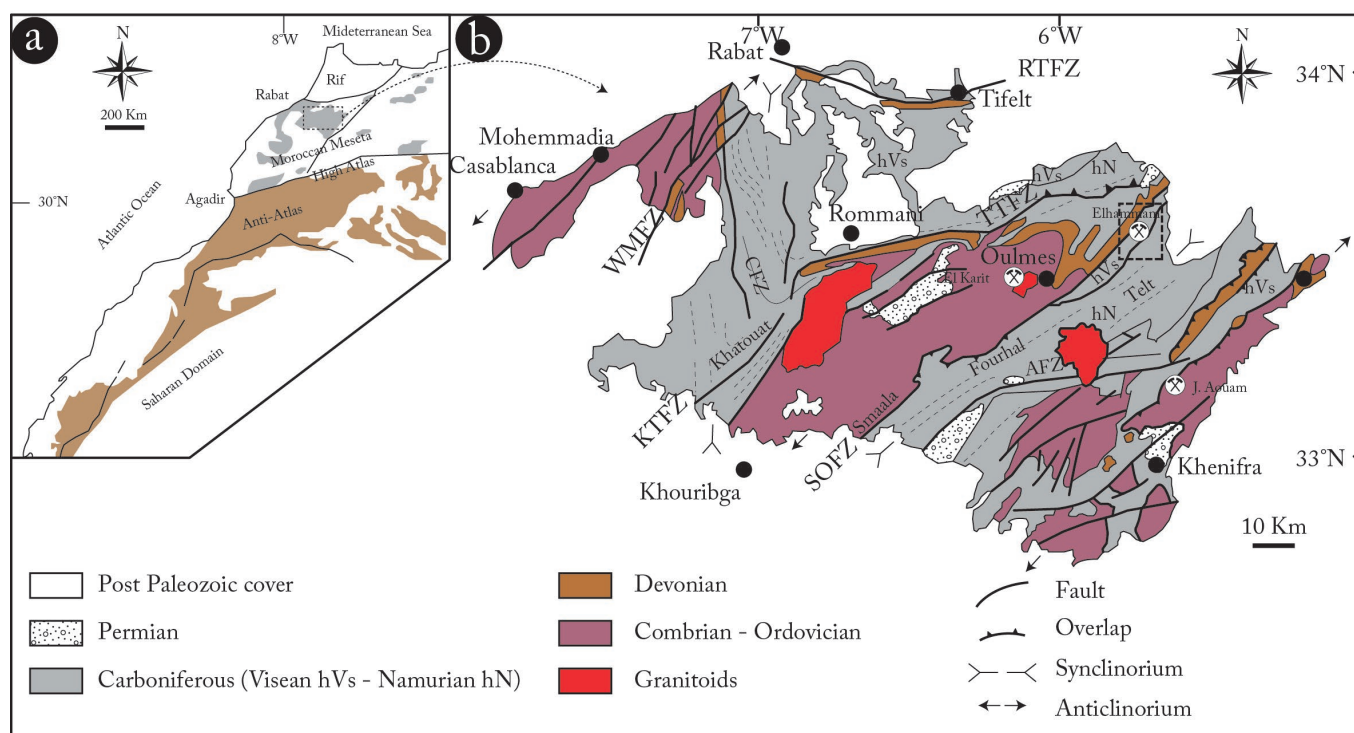
Figure 1. Map of the structural domains of Morocco and location of the Central Morocco domain (**a**) and main structural units [1,2] (**b**). (WMSZ: West Mestian Shear Zone, RTFZ: Rabat-Tifelt Fault Zone, SOFZ: Smaala-Oulmes Fault Zone, TTFZ: Tsili-Tfoudeit Fault Zone, AFZ: Aguelmous Fault Zone, KTFZ: Kef Tallal Fault Zone, CFZ: Cherrat Fault Zone).

Several studies have been carried out on these magmatic formations to establish their emplacement mode and to characterize the petrogenetic processes responsible for their formation [3–10]. The findings of these works have generated a scientific debate, to which we will return during the discussion of the results of this work, whose objectives are: (i) to define the chemical and mineralogical characteristics of the various terminal carboniferous magmatic facies of the NNE area of Achemmach, and (ii) to determine the place and the significance of the magmatism of this area in the geodynamic evolution models proposed for the interpretation of the Moroccane Hercynian chain evolution during the terminal carboniferous.
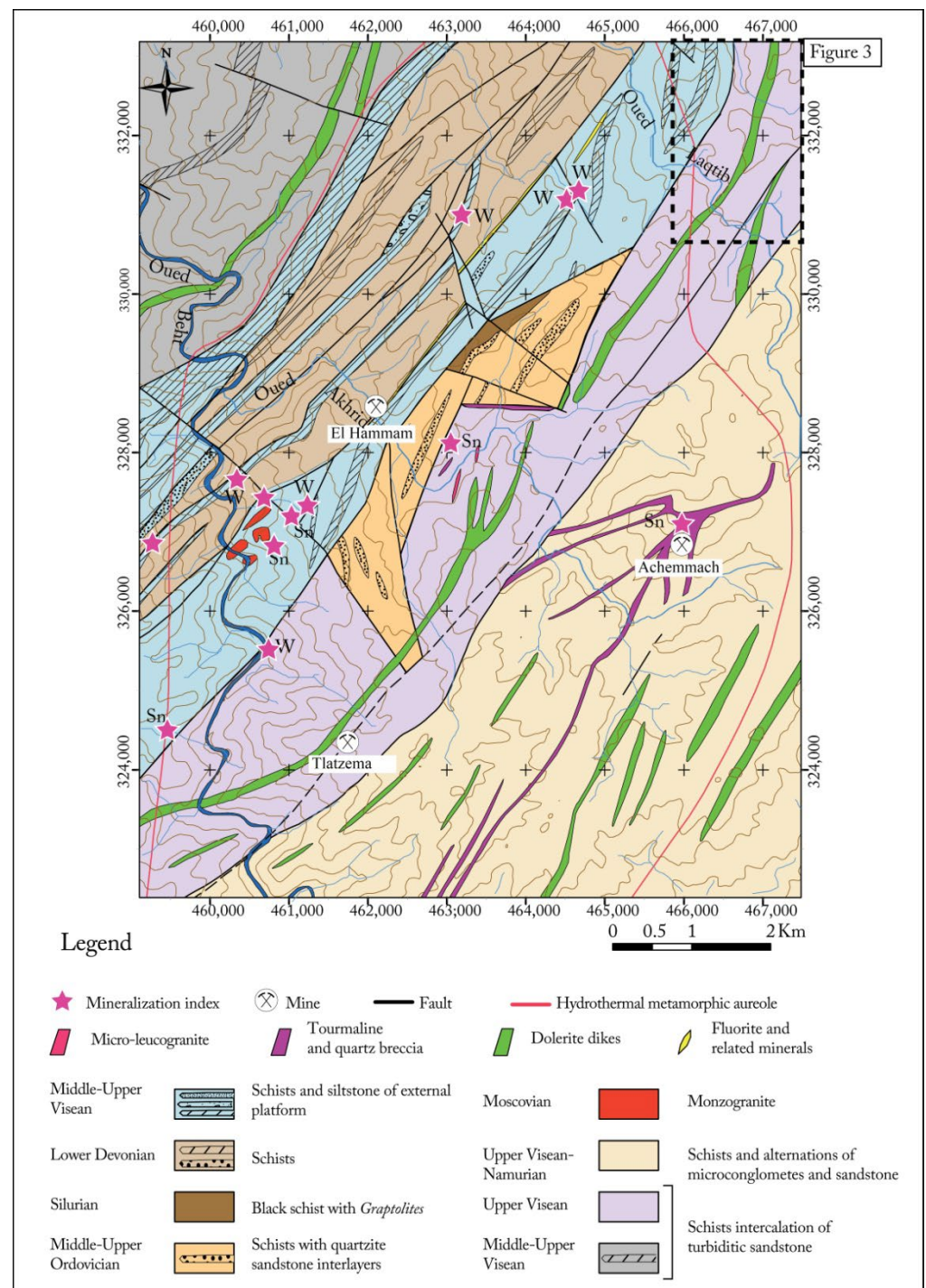
Figure 2. Geological map of the Achemmach-El Hammam district [11], displaying the location of the area under study. Sn: Tin, W: Tungsten.

2. Geological Setting

2.1. Regional Geology

The MHCM, to which the NNE sector of Achemmach belongs, consists of areduced and local Neoproterozoic basement of the palaezoic series, represented by acidic and intermediate lavas (rhyolites and andesites, respectively), granites [12], Palaeozoic terranes (Cambrian to Permian) and Meso-Cenozoic cover. The Cambrian formations are composed of carbonates platform and volcano-detritic sediments. The Ordovician is represented by

detrital deposits (shales, sandstones and quartzites) in a shallow marine platform-type environment [13]. The Silurian is characterized by a glacio-eustatic transgression, giving black graptolitic pelites and carbonates. The Devonian (Lower and Middle Devonian) is dominated by clay and carbonate minerals of reef deposits [2,14–23].

The Eovariscan deformation (Devono-Dinantian) is responsible for the formation of Sidi Bettache and Azrou-Khenifra basins, first as a pull-apart controlled by NNE-SSW to NE-SW border offsets, the second as a foreland basin-type whose creation and development are controlled by WNW propagation of thrust-related folds [11,15,18,20,21,24–27]. Carboniferous sedimentation is mainly represented by the Visean-Namurian deposits. In central Morocco, the Visean is made up of a thick detrital and carbonate series [11,14,17–19,26,28–30], showing conglomerates, schists and limestones followed by sandstone and pelitic formations. The Namurian is mainly composed of flyschs [11,29]. These Visaan and Namurian deposits are associated with magmatic mafic rocks represented by sills, dykes and lavas (basalts, dolerites and gabbros) [4,8,14,25,31–33]; this magmatism has been described by several authors. Some of them have attributed a transitional alkaline to the tholeiitic affinity of these rocks [4], other authors attributed a calc-alkaline tendency to them on the basis of the NE of the Fourhal region mafic rocks studies [8].

Lower Permian (Autunian) deposits are represented by conglomerates, sandstones, siltstones and cinerites in intra-continental basins, and are associated with significant calc-alkaline volcanism (trachytes, andesites and rhyolites) [21,33–38].

The post-Palaeozoic cover begins with Triassic formations represented by conglomerates, sandstones, red argillites and dolerite basalts [39–42]. These are dated from 201.7 ± 2 to 197.8 ± 0.7 Ma [42]. Developed rather south of the massif, Upper Cretaceous deposits are represented by marls and limestones [1]. At the end of the Upper Cretaceous and the Eocene, phosphate layers were formed.

The major Hercynian deformation (Upper Westphalian-Stephanian), dated between 300 Ma and 290 Ma [43], is due to NW-SE compression, and has structured the Massif Central into anticlinorial and synclinorial units, oriented NE-SW [1,15,18,21]. These are separated by mega faults, including the Smaala-Oulmes Fault Zone (SOFZ), which extends from the Smaala in the south [34,44,45] to beyond the district of El Hammam in the north [11,29,32,46]. These structural units show syn-schist folds, generally oriented to the SE and locally to the NW, with associated overlaps and thrusts [21]. In this Mesetian domain, syn-orogenic granitic plutons [47–51] are calcareous and mostly peraluminous [52–54].

2.2. Local Geology—Field Work

Locally, the NNE sector of Achemmach consists of two Paleozoic sets that make up the bulk of the outcropping rocks [55] (Figure 3):

- A metasedimentary complex consists of two units: (i) a calcareous and schisto-sandstone unit of middle to upper Visean age. It has an overall NE-SW direction with a dip average of 60° to 70° towards the NW (Figures 8e and 9). This unit begins with limestones alternating with schists and continues with schists, sandstones and greenish pelites where a decametric horizon of pillow-lavas is interspersed towards the north. Towards the south, the series ends with alternating shales and sandstones and more or less sandy slate schists and (ii) a flyshoid unit, by analogy with the work of [29] on the Palaeozoic of the Agourai region; this series is attributed to the Upper Visean-Namurian. This is based on a series composed by limestone, schist, sandstone and volcanic rocks of the Middle to Upper Visean through a tectonic contact corresponding to the NE-SW to NNE-SSW overlapping shear zone of Ticht-Ougas (Figure 3). This formation begins with granoclassified microconglomerates and continues with rhythmic alternations of pelites and sandstone topped by a sandstone bar. No magmatic rocks associated with this formation are known in the area under study. Despite the effects of Hercynian tectonics (succession of metric, decametric and hectometric folds), the lithostratigraphic column of this series can be reconstituted as a whole (Figure 4). It is formed by a rhythmic alternation of sandstone and pelites

several hundred meters thick. The determination of the precise strength of the series is nearly impossible because of the intensity of the Hercynian deformation and by the quaternary alluvial cover (Figure 4). The lithostratigraphic logs in Figure 5 provide a synthetic description of these two units for both the southern and northern parts of the studied area.

- A magmatic complex is materialized by volcanic (pillow-lavas), hypo-volcanic (dolerites) and plutonic (olivine-bearing gabbros) rocks (Figure 3). Thus, according to their mode of emplacement and relative chronology, petrography and structural characteristics, three types are distinguished: (i) pillow-lavas of greenish to dark green color (Figure 12, outcropping about 150m west of the sector (Figure 3). They occur in a continuous decametric horizon (20 to 25 m) with an overall direction of N25° to N30° E. They are offset in places by transverse faults N130 to N165° E (Figure 3). Their global direction, NE-SW (in the south) to N-S (in the north), is parallel to the stratification direction of the surrounding pelites with a dip to the NW in the south and to the west in the north (Figure 9). These basic lavas are embedded in a facies of greenish pelites (Figure 3). At the outcrop, they are easily recognizable thanks to their petrographic facies (texture and presence of calcite-filled vacuoles) and the presence of obvious pillow shapes (Figure 13a–d). They constitute ahorizon formed by a stack of decimetric to metric cushions, with fixed edges, and showing radial fractures. Some pillow edges are drawn by fine pelitic (greenish) sedimentary intercalations, probably indicating repeated volcanic activity in brief episodes. These lavas showa large vacuole distribution heterogeneity (resulting from the degassing of the lava) filled with late calcite. There is also a lateral variation in the proportion and size of the vacuoles (Figure 13a,b). From the center toward the edge, there is an evolution with levels very rich in vacuoles to others that are less rich or even devoid of them. (ii) Deformed, metamorphosed and altered dolerites occur as dikes intruding shales, sandstones and pelites of the supra-calcareous series of Middle to Upper Visean age; they have an overall NE-SW direction with a north-west dip (Figures 3 and 9). Their thickness is highly variable, ranging from less than 0.5 m to more than 15 m. Two criteria qualify these magmatic bodies as dikes: their overall direction is not in conformity with the stratification (Figure 14) and the thermal effect that these dikes develop, when their thickness is important, results in a more or less intense silicification at the level of the contacts with the schists and the schisto-sandy-calcareous rocks that are in contact with the surrounding shales and schisto-sandy-calcareous rocks (Figure 14). In some cases, we note that the wall of these bodies corresponds to a tectonic breccia of 30 to 60 cm of thickness, which shows that their emplacement is controlled by early faults (Figure 14). The majority of these dolerites are affected by a very penetrating flow schistosity, whose overall direction is consistent with that of host rocks (major schistosity). At the outcrop, these dolerites are highly altered with reddish patina, which is attributed to iron oxides in supergenic alteration. In addition, (iii) olivine-bearing gabbros outcrop in dikes of variable thickness and intrude on the supra-calcareous schisto-sandy series (Figure 3). These dikes are not affected by the schistosity of the major phase and would postdate this phase [55].

At the end of the Devono-Dinantian extension, and after the filling of the Visean basins, the regime of constraints that had been extensive (NW-SE) changed and became compressive, announcing the Hercynian orogenesis.

The Middle-Upper Visean and Upper Visean–Namurian terranes are affected by the major phase of Hercynian orogenesis. It is responsible for a syn-schistose folding under conditions of epizonal metamorphism (facies of green shales with sericite-chlorite). This orogenesis is marked at first by a major episode of ductile deformation (folding) followed by episodes of brittle deformation (fracturing and fault development). In El Hammam district and the Paleozoic formation of the Agourai region as a whole, the Hercynian orogenesis is responsible for the major NE-SW structuring in synclines and anticlines [29,46]. The maximum constraint responsible for this structuring is broadly NW-SE-oriented (Figure 6).
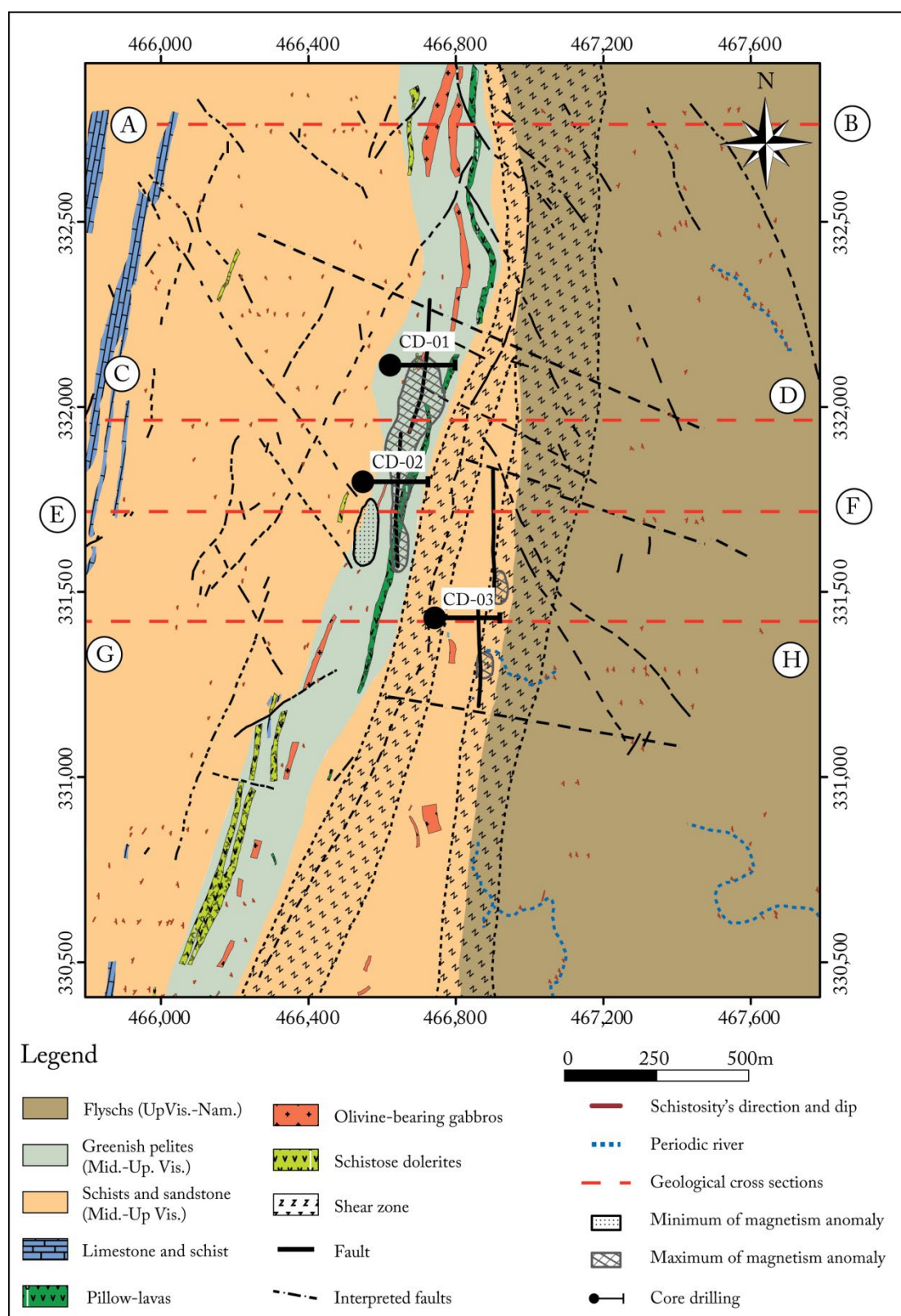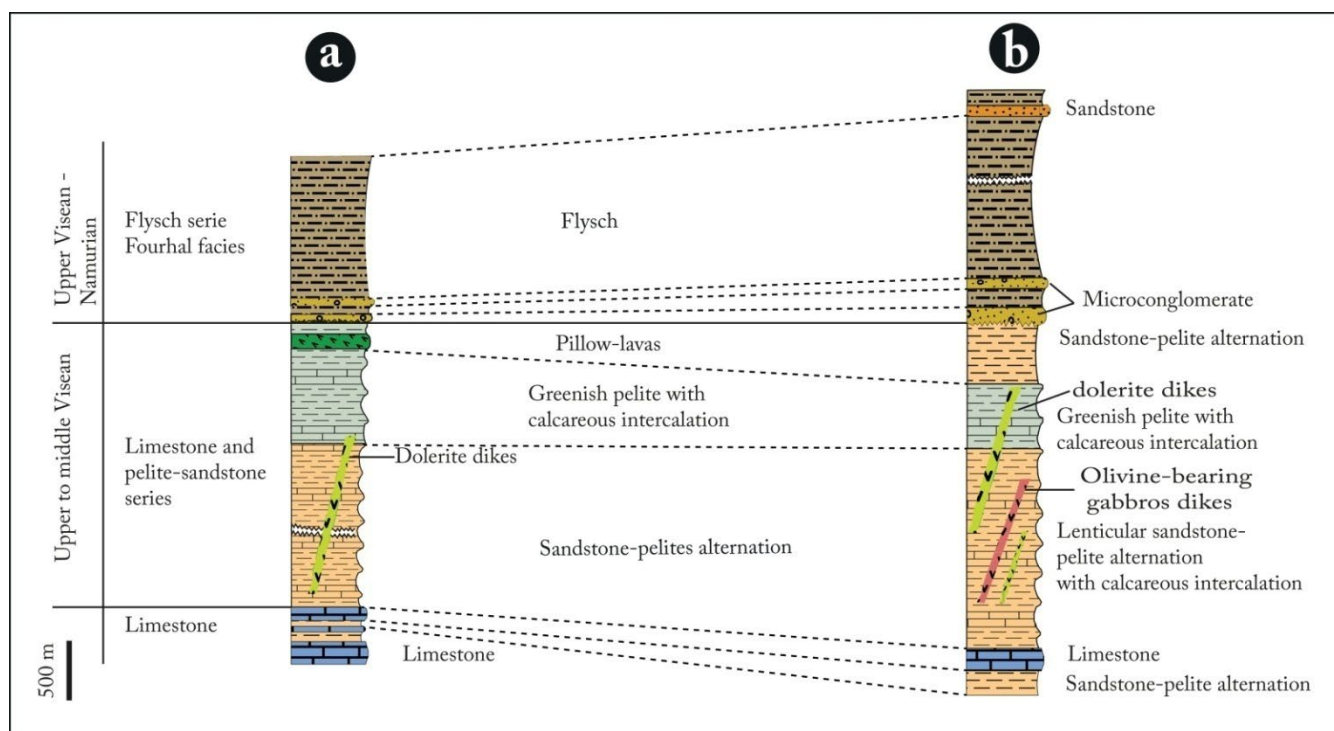
Figure 3. Geological map of the NNE Achemmach. (Mid.-UpVis.—Middle-Upper Visean, UpVis-Nam.—Upper Visean-Namurian). A–H: position of the geological sections.
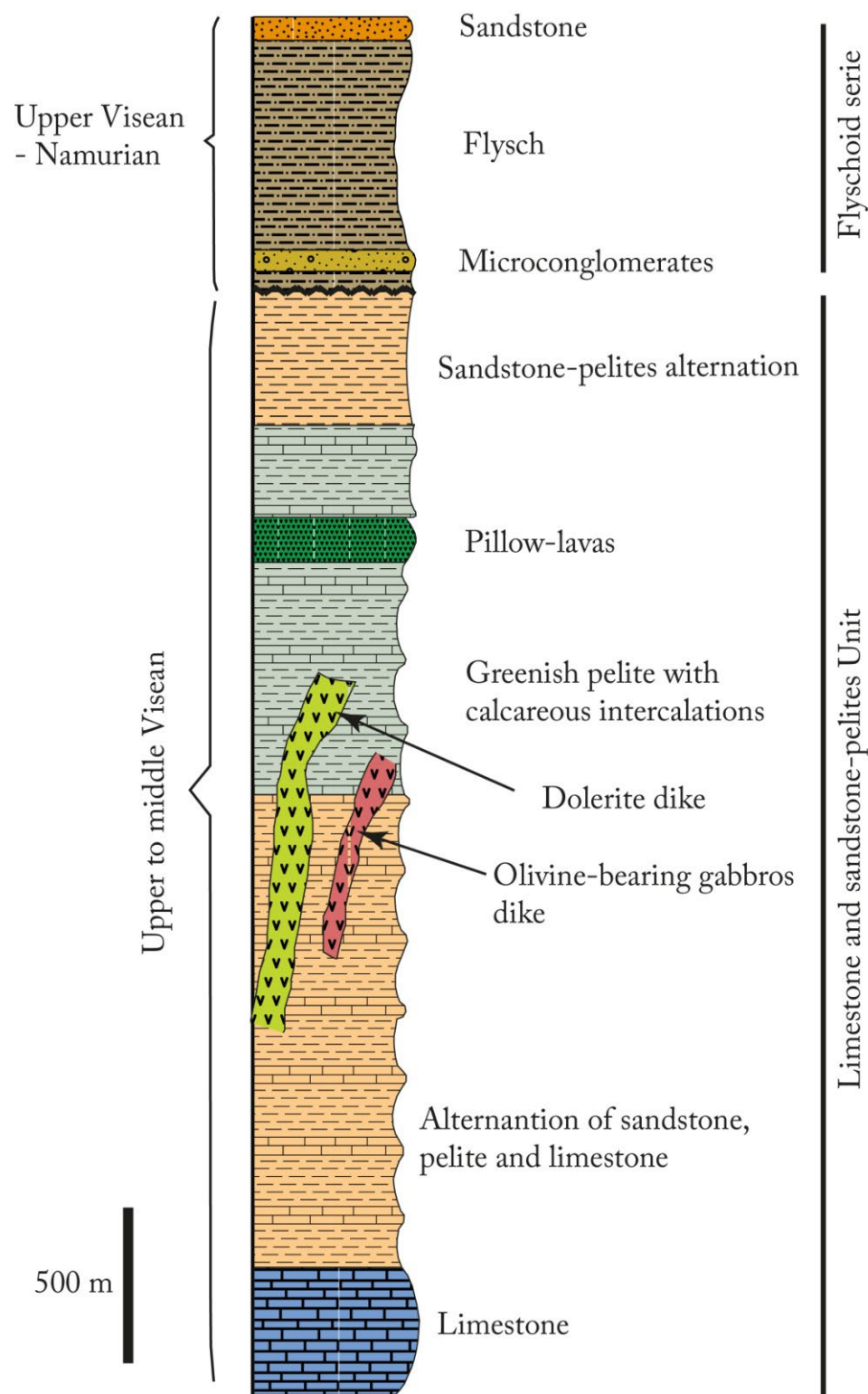
**Figure 4.** Synthetic lithostratigraphic column of the NNE Achemmach.

Figure 5. Correlation betweensynthetic lithostratigraphic logs of the southern (**a**) andnorthern (**b**) sectors of study area.

All of the western zone terranes (except the gabbros) are affected by a very penetrating flow schistosity. This S1 schistosity shows an overall NE-SW direction in the south to NNE-SSW or even N-S in the north of the area. This zone seems, according to the schistosity-stratification relations, to present a large synformal structure with metric isoclinal and synschist (P1) folds. The axes of these folds are oriented N20° to N25° E and their axial planes dip 60–70° to the NW; consequently, these folds are tilted to the SE (Figure 8e). The S1 schistosity associated with the P1 folds expands both in metasedimentary rocks and in early volcanic and hypovolcanic rocks (dolerites).

All the formations in the western zone have an overall direction of NE-SW in the south to NNE-SSW in the north, and their dip is always NW and WNW with a value that is relatively strong varying between 50° and 80°. It is important to note that some outcrops have a very shallow dip, which we attribute to the mowing of the structures due to slope effects [55].

The E-W geological sections in Figure 9 show the general structure of this area. The S1schistosity, associated with the folding of the major phase (P1), is a flow schistosity that is very penetrating; it has a NE-SW direction in the south of the zone and NNE-SSW to the N-S direction in the north of the zone. Its dip varies between 40° and 80° NW. It is slightly oblique at an angle of 5° to 10° with respect to the stratification (Figure 8e). The schistosity (S1) affects the dolerite dikes, giving them a cut appearance (especially in a fine facies) (see further in Figure 14). Unlike sedimentary formations, the dolerite dikes do not show significant folding. This is probably due to the orientation of their NE-SW direction (Devono-Dinantian extension), which is almost orthogonal to the maximum constraint. Therefore, these dikes are not folded but are schistose (flattened). The pillow-lavas horizon is also affected by this schistosity (S1). It exhibits a schistose flow parallel to S1 of the surrounding sedimentary rocks. It is also observed that the calcite vacuoles display a mineralogical lineage parallel to the major schistosity.
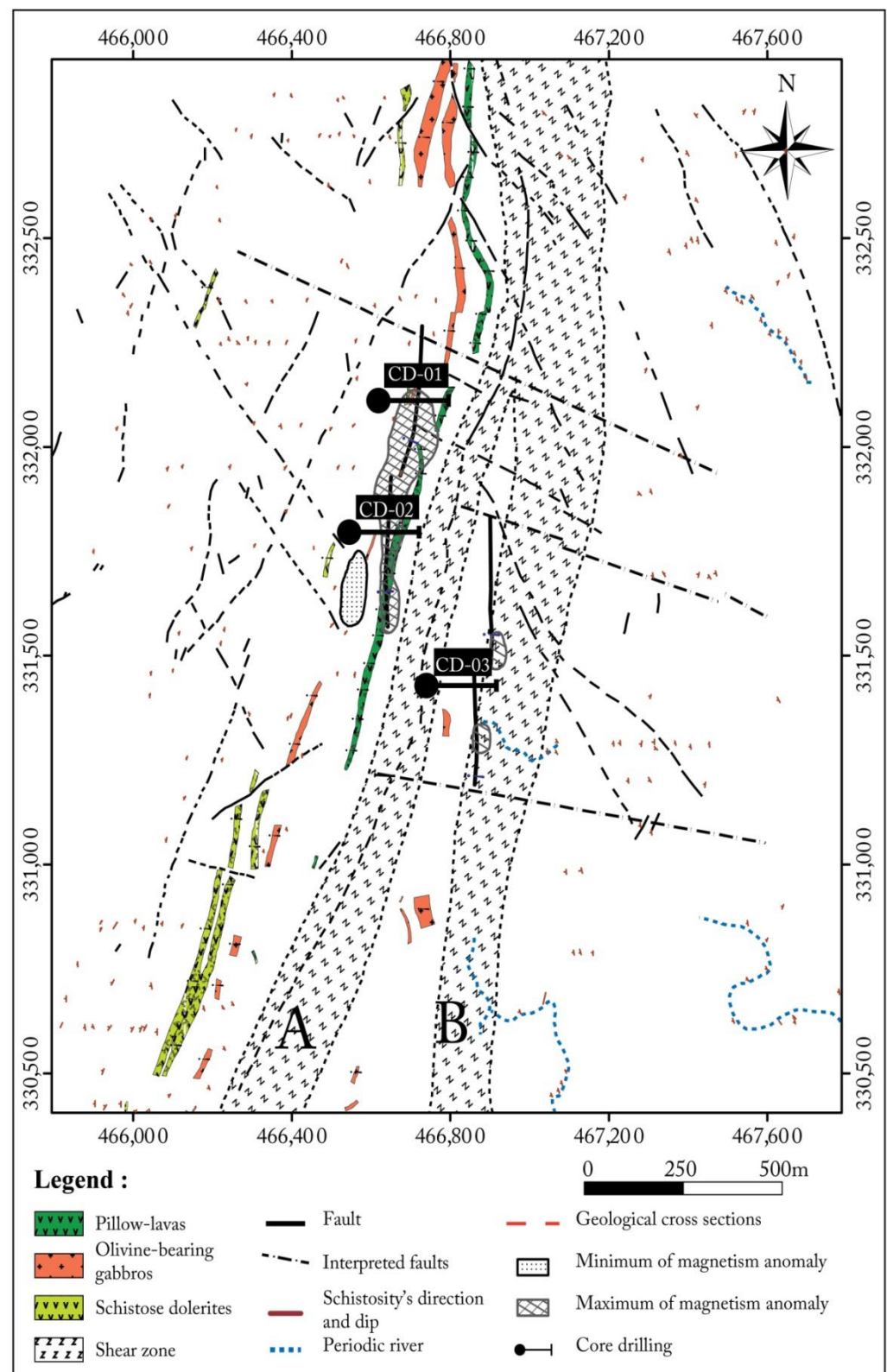
Figure 6. Structural map of the NNE Achemmach. A and B: schears zones.

The metasedimentary formations in the western zone are locally affected by intense microfolding. These folds have subvertical axes in the N165° to N150° E axial planes. The axes often plunge 80° to 85° to the NW. These folds are sometimes associated with a schistosity of the axial plane, N165° to N165° (Figure 7b,c); they occur in the finely

alternating series of pelites and sandstones, and especially near to shear zones. They are Z-shaped microfolds associated with dexterous shear gaps. This micro-folding affected the terrain after the major schistosity (S1). Locally, this microfolding can be developed in certain fine dolerite dikes. This is the case in the south of the sector at Oued Bergamou.

The schistosity (S2) is a non-penetrative flow schistosity that can be observed locally. It has been identified in the western part of the sector, basically close to the shear zone. It is well expressed in greenish pelites hosting the pillow-lavas. It presents an overall direction of N30° to N45° E (Figure 7c), always with a slight dip (varies between 30° and 45°) towards the north-west. It intersects S1, giving a flow of rhombic fries in the affected formations. The planes of schistosity S2 are relatively spaced (1 to 2 cm) but are well marked as they approach the Ticht-Ugandaas shear zone. The S2 schistosity seems to develop in relation to the overlapping of the western part on the eastern part (flysch) following an overlapping shear deformation.

The diagram in Figure 11 displays an interpretative picture of the structure of the western zone. The latter is based on the schistosity-stratification relationships and the direction of the polarity of the formations.

The flyschoid series constitute the bulk of the formations in the studied area. They are affected by the major phase of Hercynian tectonics. The latter develops folds at different scales: hectometric, decametric and metric on the NE-SW axes, in the south of the sector to NNE-SSW and even N-S in the north. These folds are all discharged towards the SE or towards the East. The large hectometric fold structures contain both decametric and metric folds (Figure 8a,b).

The metric folds (Figures 8a and 9) are synschist and isoclinals with more or less pointed hinges, which are folded in a SE or E direction. The axial schistosity (S1) exhibits a refraction phenomenon at the level of the sandstone layers. These folds always have an axial plunge of 20° to 25° to the SW or to the NE at the level of the hinges of the decametric folds affecting the microconglomeratic layer; one notes the abundance of quartz extrados slits of power ranging from 2 to 15 cm. The diagram in Figure 11 shows a synthetic section showing the structure of the eastern zone of the sector [55].

The tectonic study carried out in the NNE Achemmach sector has revealed at least three episodes of brittle deformation (or even brittle-ductile deformation for some authors [30,47,56] following the major phase of Hercynian tectonics:

➢ Shear zones (Figures 6 and 10a)

The supra-limestone series arein abnormal contact with the flyschoid series (Fourhal facies) via a NE-SW to N-S shear zone. The analysis of Figure 6 shows the existence of two major shear zones (A and B) [55], both located between the west zone and the east zone. The two NE-SW shear zones to the south of the sector converge towards the north, marking a change of the NE-SW structures to the south, and becoming NN-SSW to N-S to the north of the sector (Figure 6).

Shear zone A (Figure 6) affects the terrain of the supercalcareous series to the south of the sector. It is about 150 m wide on average and is a dexterous shear zone (Figure 10d), where the shear planes are materialized by iron oxides and have deformed quartz slits. It is a zone that shows a clear difference between the dip of its lands located to the west (shallow dip) and those located to the east (fairly steep dip). This difference in dip, combined with the presence of schistosity and micro-folds with horizontal axes, indicates that it has played an overlapping role. This overlap is clearly visible to the north of the area. Thus, after the major phase, there would be an overlap of the western part over the eastern part until this phenomenon was blocked, following a change in the direction of the constraints that would have caused the zone in shear play to evolve.

Shear zone B (Figure 6) extends NE-SW to the south and becomes NNE-SSW to the north where it converges to zone A. It is an area about 200 m wide, materialized by shear planes with dextral sets, microfolds with subvertical axes, quartz lenses (in slits) and by zones of iron oxide breccia (Figure 10c). Despite the scarcity of outcrops in this zone, we can note locally (southward) the presence of microfolds with subhorizontal axes similar to

those of zone A. This shear zone involves both the west supercalcareous series and the east flyschoid series.
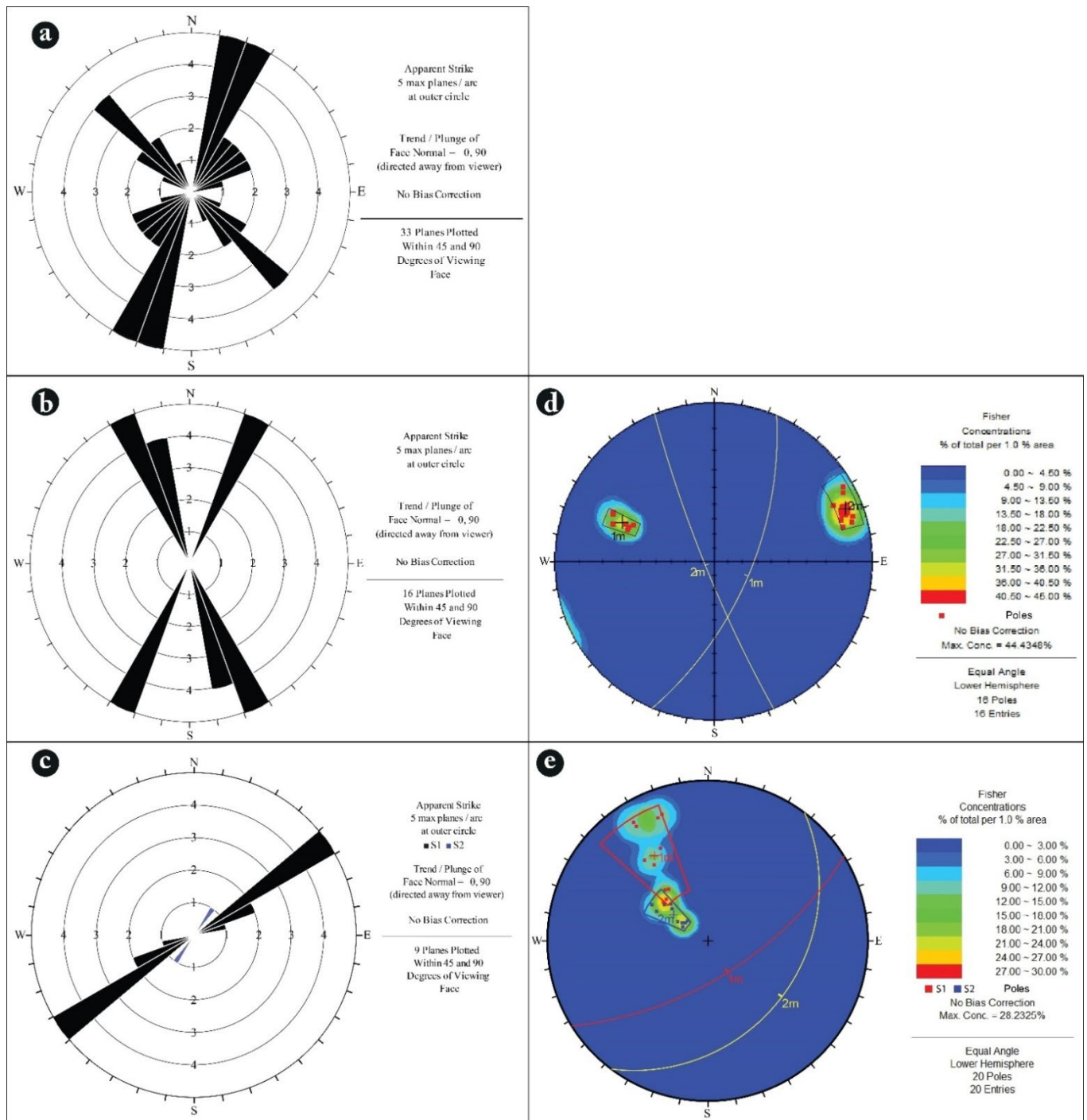
Figure 7. Directional rise in the NNE Achemmachof fault families (**a**) and fold families (**b**,**c**), and S1–S2 schistosity pole stereograms (**d**,**e**).
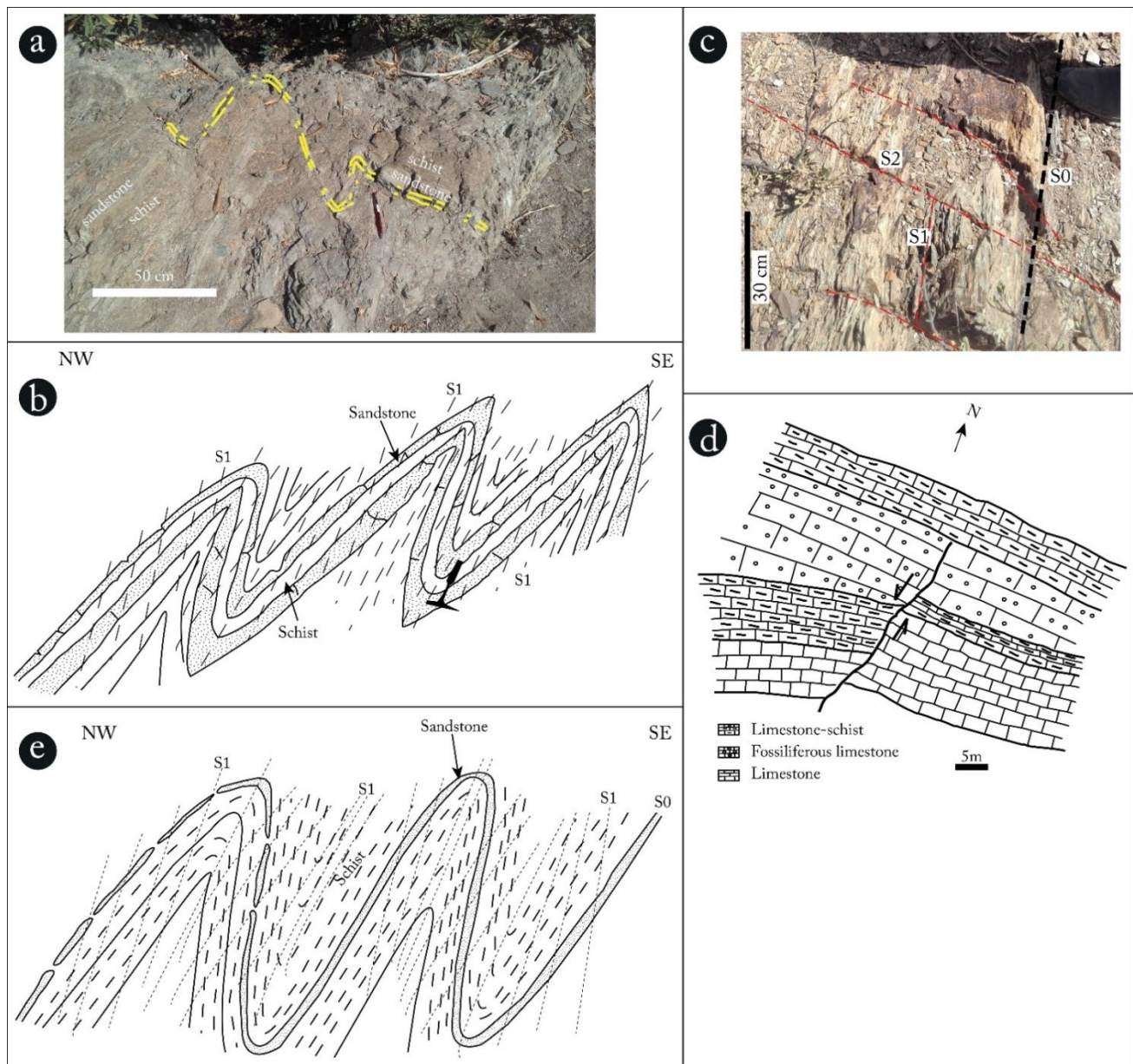
Figure 8. Folding types in the NNE Achemmach: (**a**,**b**) N-S synschist metric folds with eastern vergence of the flysch series, (**c**) relationship between schistosity and stratification (**d**) syn-sedimentary normal fault in a limestone bench of the Bergamou limestone bar (northern part of the studied area), and (**e**) NE-SW metric folds with SE vergence of the supra-calcareous schisto-sandstone formation.

➢   NE-SW to NNE-SSW faults

These faults are broadly parallel to the major schirtosity(S1) affecting all terrains study area. They are materialized in most cases by injections of quartz sub-parallel to the S1 schistosity, and are powerful from a few centimeters to about 1 m. They are subvertical faults, with an average dip of 80° NW or WNW, and always with dexter play. The absence of direct relations between these faults and the overlap does not allow us to establish their chronology. However, we believe that these faults occurred at the same time and would correspond to a common deformation episode.

1.   N10° to N50 ° E faults (Figures 6 and 7a)

They affect both the Upper-Middle Visean terrain in the western zone and the Upper Visean-Namurian terrain (flyschs) in the eastern zone of the sector (Figure 6).

In the West zone, the most important of these faults outcrops in the Oued Bergamou to the south of the sector. It affects schistose limestones and a dolerite dike. It is oriented N70° with a dip of 70° NNW. It is materialized by a breach with schist, schisto-limestones and dolerite elements, powerful of about 1m and with dexter play. On the plane of this fault, there are Fe-oxide veins and cubic cavities probably corresponding to traces of pyrite crystals.

In the eastern zone, a fault oriented N65° with a dip of 70° NNW affects the flysch series to the south. It is marked by a breach with schist and sandstone elements with local quartz and pyritein late fractures.

2.   N130° to N150° E faults

These faults werefirstly detected by a geophysical investigation [56] and confirmed laterby the geological survey. They have a large extension: 400 to 600 m, and affect the Middle Visean-Namurien terrains (Figures 6 and 7a).

To the north of the sector, there is a fault of this family, oriented N145, which shows a clear shift, in the sinistral play, of the horizon of pillow basalts and the NE-SW shear zone. These faults are materialized by breccias and quartz gashes injections (Figure 10b). Another N130° E fault affects the N70° E gabbros' dike and intersects two other faults: N55° E (NE-SW family) (Figure 11) and N0 (N-S family). N110° E to N120°E are other faults (the less important can be included in this category (Figure 7a).
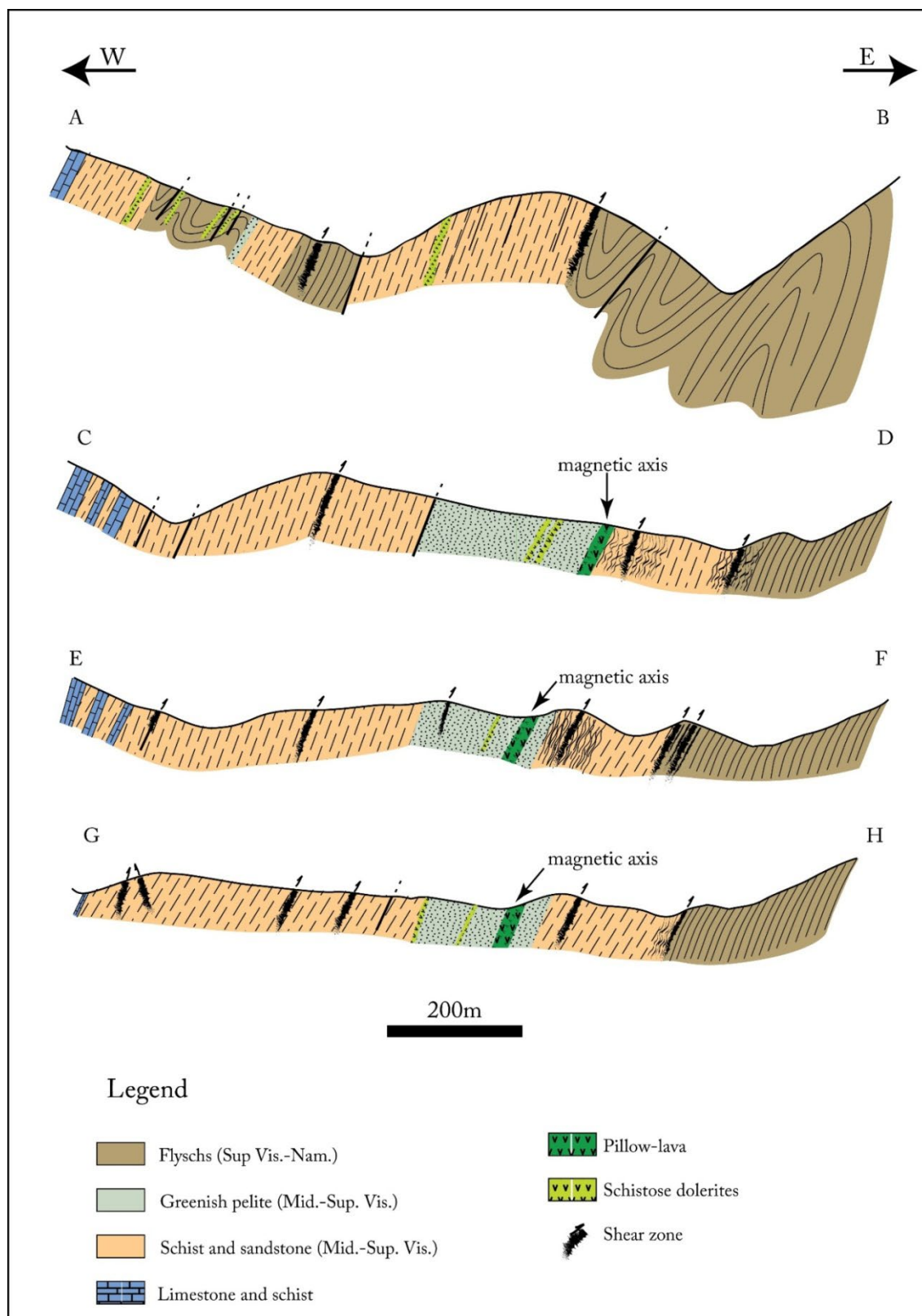
Figure 9. E-W geological sections (AB, CD, EF and GH) of the NNE Achemmach. See cross-section position in Figure 3.
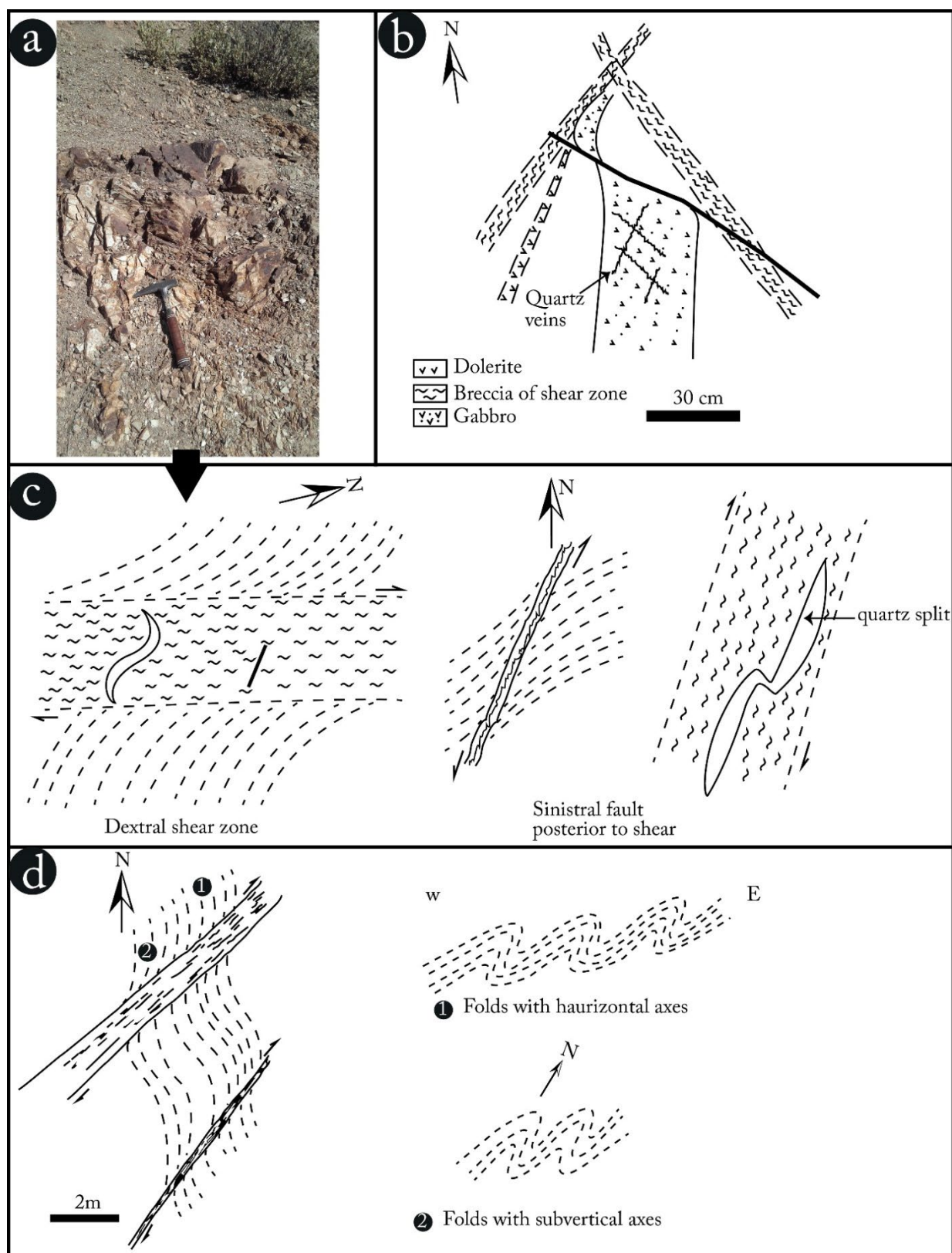
Figure 10. (**a**) Breccia in shear zone A (north of the studied zone), (**b**) N130° E sinistral fault in dolerite dike, (**c**) shear zone deformation in zone B and (**d**) shear zone deformation in Zone A.
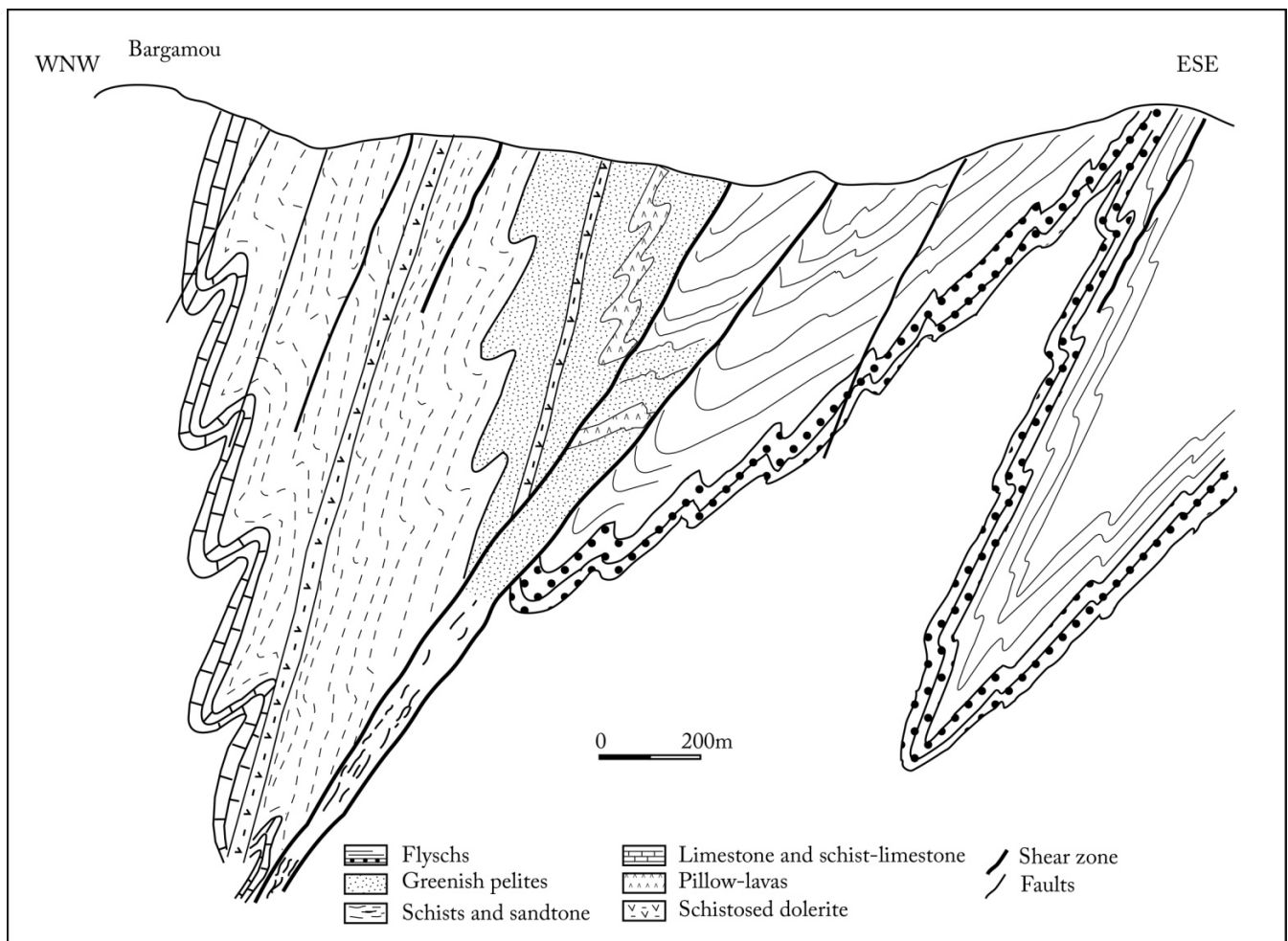
Figure 11. WNW-ESE section interpreting the structure of the NNE Achemmach [55].

3. Sampling and Methods of Analysis

The petrographic study carried out in this work is based on macroscopic and microscopic observations of about 100 representative samples of the different magmatic rock-types recognized in the NNE Achemmach sector. They are sampled both at the surface and at depth in the core holes drilled there. In order to classify our rocks and to understand the behavior of some chemical elements, we performed total rock analyses (major elements, traces, and rare earths) on 58 samples considered representative (26 pillow-lavas samples, 15 dolerite samples, and 17 olivine–gabbros samples) (Figure 6). The analyses of major elements were carried out by ICP-AES and X-ray fluorescence methods, and of trace elements and rare earth elements by the ICP-MS method at the Reminex/Managem research and development center. Chemical analyses of the samples are reported in Tables 1–3.

Table 1. Chemical analyses of the major, trace and rare earth elements of interstratified pillow-lavas in the Upper Carboniferous series of the NNE Achemmach. bdl: below detection limit. Sp.Pillow-lavas: splitized pillow lavas.

Sample	BA5	BA6	BA7	BA17	BA21	BA25	BA28	BA30	BA2	BA3	BA4	BA13	BA14	BA15	BA16	BA18	BA19	BA20	BA22	BA23	BA24	BA26	BA27	BA29	BA31	BA32
Facies	Pillow-Lavas															Sp. Pillow-Lavas										
(%)																										
SiO_2	43.8	46.07	49.51	46	48.2	53.03	45.79	45.86	42.49	42.44	42.95	45.15	42.69	41.33	48.94	46.11	45.5	47.82	44.49	50.83	48.6	46.54	40.38	44.16	48.34	48.01
TiO_2	2.74	3	2.56	2.59	2.54	2.46	2.62	2.6	2.71	2.7	2.79	2.2	2.43	2.29	2.17	2.18	2.41	2.33	2.48	2.03	2.23	2.08	2.52	2.56	2.8	2.67
Al_2O_3	17.34	16.42	16.13	16.98	16.41	15.56	17.32	16.87	17.75	17.95	18.02	14.37	15.43	14.72	14.03	14.55	15.32	15.36	16.58	13.09	16.45	13.32	16.32	17.17	14.5	14.17
Fe_2O_3	8.94	9.14	8.01	7.9	8.07	8.51	7.49	7.58	10.1	10.71	9.73	6.94	6.79	6.56	7.08	7.28	8.08	8.19	9.08	7.49	8.04	7.26	9.04	9.33	8.38	8.03
MnO	0.12	0.11	0.10	0.11	0.10	0.09	0.13	0.11	0.12	0.10	0.12	0.13	0.15	0.14	0.08	0.10	0.12	0.10	0.09	0.09	0.07	0.12	0.11	0.13	0.11	
MgO	5.15	4.65	5.14	6.03	6.67	5.33	7.73	7.84	5.29	5.88	5.86	5.27	4.86	4.34	6.14	5.20	5.97	5.66	5.72	5.84	5.40	5.02	5.96	7.51	6.08	6.24
CaO	9.67	7.26	6.87	9.73	6.29	7.99	6.23	7.88	9.27	6.84	7.68	11.06	13.23	14.74	8.03	11.54	9.52	7.29	8.23	7.67	6.63	11.83	12.38	6.86	7.78	7.6
Na_2O	5.29	5.27	5.68	5.05	4.37	4.47	4.27	4.36	4.84	5.08	5.01	4.38	3.92	3.61	5.09	4.34	4.12	3.92	4.21	4.13	4.48	3.92	4.18	4.37	4.21	4.44
K_2O	0.52	1.06	0.72	0.49	0.88	1.21	0.54	0.53	0.69	0.68	0.52	1.47	2.28	2.40	0.43	0.95	1.69	1.15	1.14	1.37	1.28	1.16	1.38	0.62	0.59	0.59
P_2O_5	1.44	1.50	1.45	1.43	1.29	1.25	1.26	1.36	1.59	1.57	1.29	1.34	1.43	1.39	1.55	1.43	1.64	1.53	1.38	1.60	1.40	1.22	1.39	1.42	1.69	1.75
LOI	5.23	3.66	4.13	4.09	4.26	4.21	5.11	3.67	5.80	6.34	6.65	8.56	6.83	7.63	7.92	7.07	5.89	8.04	7.63	7.97	6.64	8.20	6.41	6.58	5.69	7.19
Total	100.24	101.14	100.30	100.40	100.28	100.67	100.94	100.56	100.65	100.29	100.62	100.87	100.04	99.15	101.46	100.75	100.26	101.39	101.03	101.47	100.62	100.67	100.10	100.69	100.19	100.80
(ppm)																										
Ti	16,440	18,000	15,360	15,540	15,240	14,760	15,720	15,600	16,260	16,200	16,740	13,200	14,580	13,740	13,020	13,080	14,460	13,980	14,880	12,180	13,380	12,480	15,120	15,360	16,800	16,020
K	4316	8798	5976	4067	7304	10043	4482	4399	5727	5644	4316	12201	18924	19920	3569	7885	14027	9545	9462	11371	10624	9628	11454	5146	4897	4897
P	6287.04	6549.00	6330.70	6243.38	5632.14	5457.50	5501.16	5937.76	6941.94	6854.62	5632.14	5850.44	6243.38	6068.74	6767.30	6243.38	7160.24	6679.98	6025.08	6985.60	6112.40	5326.52	6068.74	6199.72	7378.54	7640.50
Ba	405	637	543	300	304	362	152	172	537	557	57	347	574	582	55	157	505	364	371	404	347	369	434	163	170	174
Rb	8.03	11.92	6.54	4.90	10.29	10.57	6.83	7.51	10.83	9.69	7.56	14.03	22.07	23.66	4.28	8.89	15.20	20.41	10.45	13.05	10.05	11.24	10.90	8.25	8.31	8.47
Sr	291	409	401	305	486	515	555	497	382	339	276	378	426	389	283	300	587	451	424	448	515	523	535	500	551	445
Cr	105	100	125	108	130	111	134	145	101	111	114	108	101	94	90	108	108	129	105	88	113	98	114	122	130	130
Ni	60	42	60	60	91	83	104	105	84	91	53	70	57	54	60	66	88	90	70	79	72	102	107	112	98	92
Cu	57	52	62	21	38	34	31	42	60	160	40	43	39	15	31	48	23	35	37	48	59	52	101	33	29	28
Zn	123	106	105	72	82	66	78	78	114	135	96	65	60	60	53	69	79	70	81	365	63	80	97	86	79	82
Sc	18.99	18.26	18.74	18.06	18.05	16.83	14.78	14.48	18.78	18.77	19.04	16	16.85	15.98	17.83	17.21	17.79	17.5	17.31	16.47	17.42	15.25	15.64	14.64	14.68	16
Li	89	80	69	51	172	bdl	200	151	163	154	166	172	90	97	143	134	46	127	150	163	206	47	90	242	79	61
Nb	17	22	23	20	18	16	20	17	25	20	23	18	17	24	22	18	16	25	21	18	17	22	25	16	15
Y	18	25	24	26	29	26	27	16	27	27	20	28	18	22	26	34	19	27	25	31	26	15	21	23	18	17
Zr	253	267	252	214	182	193	198	194	434	165	314	365	270	55	172	359	253	137	338	304	307	226	241	162	325	181
Th	2.38	2.34	2.34	2.33	2.34	2.06	1.91	1.85	2.43	2.20	2.49	2.28	2.14	1.97	2.09	2.15	2.36	2.18	2.17	2.26	2.18	1.93	2.04	1.88	1.95	2.08
La	25.95	27.78	26.49	26.53	29.33	27.97	29.24	27.87	21.69	21.72	26.61	24.53	24.57	23.62	26.85	25.59	28.50	29.37	27.78	26.49	28.02	25.99	29.78	29.24	27.83
Ce	57.60	59.51	59.24	59.79	65.56	62.84	65.54	63.50	49.61	50.10	58.56	55.88	54.72	52.93	60.59	57.85	63.96	65.05	62.86	59.28	63.67	58.16	59.24	66.13	65.56	79.69
Pr	7.06	7.20	7.24	7.23	7.85	7.49	7.83	7.66	6.19	6.27	7.20	6.69	6.66	6.43	7.33	7.00	7.69	7.73	7.51	7.09	7.60	6.98	7.10	7.94	7.83	7.63
Nd	30.16	30.66	30.78	31.44	34.33	32.71	34.07	33.53	26.69	27.23	30.46	28.54	28.83	28.00	31.77	30.42	33.50	33.72	32.90	30.89	33.13	30.27	31.13	34.70	33.96	33.23
Sm	6.42	6.45	6.51	6.30	6.82	6.39	6.69	6.52	5.92	6.01	6.47	5.88	5.90	5.70	6.38	6.10	6.60	6.63	6.48	6.19	6.53	5.95	6.13	6.80	6.60	6.50
Eu	1.86	2.04	2.12	2.11	2.09	2.18	2.07	2.08	1.59	1.59	1.84	1.87	1.94	1.92	2.11	1.98	2.26	1.94	2.16	2.10	2.22	2.03	2.05	2.26	2.24	2.15
Gd	6.85	6.80	6.82	6.69	7.18	6.80	7.01	6.89	6.28	6.37	6.87	6.16	6.28	6.05	6.74	6.47	7.01	6.99	6.90	6.56	6.93	6.33	6.49	7.14	6.90	7.00
Tb	1.17	1.15	1.15	1.25	1.35	1.28	1.30	1.29	1.06	1.07	1.16	1.09	1.15	1.11	1.24	1.22	1.33	1.31	1.31	1.23	1.31	1.22	1.24	1.34	1.30	1.32
Dy	5.92	5.83	5.84	5.87	6.09	5.84	5.84	5.72	5.56	5.41	5.95	5.47	5.54	5.26	5.86	5.70	6.12	5.92	5.95	5.77	5.94	5.48	5.68	5.95	5.74	5.90
Ho	1.32	1.29	1.30	1.44	1.52	1.45	1.41	1.39	1.21	1.15	1.31	1.27	1.35	1.26	1.41	1.42	1.55	1.47	1.48	1.43	1.49	1.39	1.45	1.43	1.40	1.46
Er	3.31	3.20	3.24	3.29	3.27	3.16	3.00	2.96	3.18	2.87	3.35	3.13	3.10	2.91	3.22	3.23	3.50	3.17	3.25	3.27	3.25	3.02	3.16	3.05	2.95	3.14
Tm	0.44	0.43	0.44	0.44	0.44	0.41	0.38	0.38	0.43	0.38	0.46	0.43	0.41	0.39	0.43	0.44	0.46	0.42	0.44	0.44	0.44	0.40	0.42	0.40	0.38	0.42
Yb	3.15	3.07	3.11	3.53	3.63	3.53	3.14	3.30	2.94	2.60	3.15	3.15	3.26	3.07	3.41	3.50	3.82	3.52	3.68	3.54	3.63	3.34	3.50	3.28	3.13	3.57
Lu	0.41	0.37	0.38	0.39	0.36	0.34	0.30	0.30	0.39	0.33	0.42	0.40	0.38	0.35	0.37	0.40	0.42	0.35	0.37	0.40	0.37	0.35	0.37	0.30	0.30	0.34
AI	27.48	31.30	31.83	30.61	41.46	34.42	44.06	40.61	29.77	35.50	33.46	30.39	29.39	26.86	33.37	27.92	35.96	37.79	35.54	37.93	37.55	28.18	30.71	41.99	35.74	36.20
ASI	0.82	0.88	0.88	0.81	1.03	0.83	1.14	0.97	0.88	1.04	1.00	0.62	0.58	0.52	0.76	0.63	0.72	0.90	0.89	0.72	0.96	0.58	0.66	1.06	0.84	0.82

Table 1. *Cont.*

Sample	BA5	BA6	BA7	BA17	BA21	BA25	BA28	BA30	BA2	BA3	BA4	BA13	BA14	BA15	BA16	BA18	BA19	BA20	BA22	BA23	BA24	BA26	BA27	BA29	BA31	BA32
Facies				Pillow-Lavas													Sp. Pillow-Lavas									
Nb/Y	0.94	0.88	0.96	0.77	0.62	0.62	0.74	1.06	0.93	0.74	1.15	0.64	0.94	1.09	0.85	0.53	0.84	0.93	0.84	0.58	0.65	1.47	1.00	1.09	0.89	0.88
Zr/Ti	0.02	0.01	0.02	0.01	0.01	0.01	0.01	0.01	0.03	0.01	0.02	0.03	0.02	0.00	0.01	0.03	0.02	0.01	0.02	0.02	0.02	0.02	0.02	0.01	0.02	0.01
Tb/Yb	0.37	0.37	0.37	0.35	0.37	0.36	0.42	0.39	0.36	0.41	0.37	0.35	0.35	0.36	0.37	0.35	0.35	0.37	0.36	0.35	0.36	0.36	0.35	0.41	0.41	0.37
La/Sm	4.04	4.31	4.07	4.21	4.30	4.38	4.37	4.27	3.66	3.62	4.11	4.17	4.16	4.15	4.21	4.19	4.32	4.43	4.29	4.28	4.29	4.37	4.30	4.38	4.43	4.28
Y/Nb	1.06	1.14	1.04	1.30	1.61	1.63	1.35	0.94	1.08	1.35	0.87	1.56	1.06	0.92	1.18	1.89	1.19	1.08	1.19	1.72	1.53	0.68	1.00	0.92	1.13	1.13

Table 2. Chemical analyses of major, trace and rare earth elements of dolerite dikes in the Upper Carboniferous series of the NNE Achemmach. bdl: below detection limit.

Sample	BA33	BA34	BA35	BA36	BA37	BA38	BA39	BA40	BA41	BA42	BA45	BA68	BA67	BA69	BA44
Facies								Dolerite							
(%)															
SiO$_2$	49.07	48.6	48.66	49.32	51.29	45.04	52.36	49.01	51.47	44.95	48.06	47.03	46.5	47.61	46.46
TiO$_2$	1.36	1.34	1.23	1.25	1.34	1.41	1.28	1.34	1.55	1.27	1.62	1.1	1.19	1.25	1.39
Al$_2$O$_3$	18.93	17.85	17.47	17.82	18.54	19.53	17.16	18.63	19.59	18.05	19.41	17.9	16.77	17.51	19.01
Fe$_2$O$_3$	11.39	12.72	11.14	12.03	11.56	12.47	10.16	10.64	12.3	9.98	14.18	10.97	11.44	13.72	14.48
MnO	0.22	0.20	0.17	0.18	0.18	0.31	0.21	0.25	0.12	0.38	0.11	0.28	0.26	0.45	0.35
MgO	10.57	12.06	9.90	10.83	10.76	11.64	9.08	9.00	12.45	8.77	13.75	14.85	9.06	12.24	12.74
CaO	7.23	6.41	8	6.51	5.21	7.05	8.83	8.1	1.79	10	0.26	3.23	9.96	6.14	5.12
Na$_2$O	0.23	0.87	1.22	1.16	0.54	0.12	0.11	1.33	0.56	1.09	0.66	1.45	1.98	0.67	0.11
K$_2$O	1.72	0.67	0.52	0.60	0.94	1.54	1.42	2.13	0.42	2.79	0.33	1.09	1.58	0.91	1.13
P$_2$O$_5$	0.17	0.18	0.15	0.18	0.16	0.17	0.17	0.18	0.17	0.15	0.17	0.11	0.16	0.15	0.17
LOI	0.10	0.07	1.37	1.05	0.12	0.09	0.11	0.13	0.42	0.39	0.22	0.35	1.47	0.09	0.08
Total	100.99	100.97	99.83	100.93	100.64	100.97	100.89	100.74	100.84	100.82	100.77	100.66	100.37	100.74	101.04
(ppm)															
Ti	8160	8040	7380	7500	8040	8460	7680	8040	9300	7620	9720	6600	7140	7500	8340
K	14276	5561	4316	4980	7802	12782	11786	17679	3486	23157	2739	9047	13114	7553	9379
P	742.22	785.88	654.90	785.88	698.56	742.22	742.22	785.88	742.22	654.90	742.22	480.26	698.56	654.90	742.22
Ba	124	89	138	204	117	306	286	348	173	368	67	141	235	45	229
Rb	17.00	15.71	17.98	15.88	15.40	12.00	16.00	18.00	15.00	16.00	11.88	15.00	16.87	12.00	14.00
Sr	367	267	321	318	309	401	481	423	401	218	291	281	345	304	403
Cr	205	197	202	189	206	205	120	110	218	114	197	244	148	207	212
Ni	71	69	88	85	80	95	72	71	99	74	94	157	66	62	71
Cu	220	43	136	78	219	85	66	58	63	106	119	87	95	110	91
Zn	93	113	73	95	101	743	225	130	183	102	101	70	101	79	92
Sc	25.59	22.28	22.24	23.22	25.2	26.67	23.58	24.73	23.94	24.39	31	22.51	28.31	32.58	24.92
Li	157	177	148	116	189	220	105	136	170	490	548	525	566	378	395
Nb	26	29	bdl	bdl	11	8	19	15	27	21	19	14	17	26	26
Y	17	16	14	14	16	16	16	16	16	17	16	12	17	16	16
Zr	206	126	155	224	174	201	150	267	212	200	128	124	175	162	129
Th	0.49	0.31	0.33	0.34	0.42	0.41	0.36	0.39	0.33	0.40	0.31	0.30	0.49	0.34	0.45
La	4.69	4.70	5.83	4.46	4.58	5.13	5.02	5.06	4.80	6.07	4.60	4.20	5.10	4.80	4.60
Ce	11.92	11.46	11.96	11.05	11.58	12.24	11.10	11.89	10.48	12.84	12.75	10.65	12.04	10.73	11.62
Pr	1.82	1.81	1.65	1.70	1.75	1.88	1.75	1.84	1.71	1.96	1.85	1.52	1.80	1.71	1.63
Nd	9.22	9.29	8.43	8.74	9.04	9.53	8.94	9.49	8.72	9.92	10.22	8.27	10.08	9.20	8.70
Sm	3.03	3.02	2.82	2.86	2.97	3.04	2.94	3.13	2.81	3.07	3.11	2.39	3.10	2.69	2.56
Eu	0.77	1.03	1.09	1.15	0.90	0.66	0.89	0.96	0.83	1.21	0.62	0.67	1.20	0.86	0.83
Gd	3.45	3.44	3.18	3.27	3.41	3.44	3.36	3.66	3.21	3.93	4.08	3.14	4.02	3.37	3.29
Tb	0.62	0.61	0.56	0.58	0.60	0.61	0.59	0.65	0.56	0.71	0.65	0.49	0.64	0.53	0.52
Dy	3.93	3.80	3.57	3.68	3.84	3.89	3.72	4.09	3.54	3.18	4.68	3.49	4.58	3.82	3.80
Ho	0.82	0.78	0.74	0.76	0.80	0.81	0.77	0.84	0.73	0.96	0.85	0.62	0.83	0.68	0.70
Er	2.38	2.23	2.12	2.19	2.31	2.38	2.25	2.48	2.09	2.53	2.42	1.81	2.39	2.01	2.05
Tm	0.33	0.31	0.29	0.30	0.33	0.34	0.31	0.34	0.29	0.35	0.25	0.25	0.33	0.28	0.30
Yb	2.17	1.91	1.87	1.97	2.08	2.21	2.00	2.23	1.84	2.50	2.37	1.79	2.43	2.06	2.13
Lu	0.30	0.26	0.26	0.27	0.30	0.31	0.35	0.32	0.26	0.25	0.29	0.23	0.30	0.26	0.27
AI	62.23	63.62	53.05	59.84	67.05	64.77	54.01	54.13	84.56	51.04	93.87	77.30	47.12	65.88	72.62
ASI	1.49	1.65	1.32	1.58	2.01	1.62	1.21	1.16	5.10	0.94	10.86	2.22	0.90	1.65	2.16
Nb/Y	1.53	1.81	-	-	0.69	0.50	1.19	0.94	1.69	1.24	1.19	1.17	1.00	1.63	1.63
Zr/Ti	0.03	0.02	0.02	0.03	0.02	0.02	0.02	0.03	0.02	0.03	0.01	0.02	0.02	0.02	0.02
Tb/Yb	0.28	0.32	0.30	0.29	0.29	0.27	0.29	0.29	0.30	0.28	0.27	0.27	0.26	0.26	0.25
La/Sm	1.55	1.56	2.07	1.56	1.54	1.69	1.71	1.62	1.71	1.98	1.48	1.75	1.65	1.78	1.80
Y/Nb	0.65	0.55	-	-	1.45	2.00	0.84	1.07	0.59	0.81	0.84	0.86	1.00	0.62	0.62

Minerals **2022**, *12*, 622
20 of 39

Table 3. Chemical analyses of the major, trace and rare earth elements of the olivine-bearing gabbros dikes in the Upper Carboniferous series of the NNE Achemmach. bdl: below detection limit.

| Sample	BA52	BA53	BA54	BA56	BA57	BA58	BA59	BA60	BA61	BA62	BA63	BA64	BA65	BA43	BA49	BA51	BA70
Facies								Olivine-Bearing Gabbros									
(%)																	
SiO$_2$	49.4	47.67	49.96	47.36	51.07	50.24	54.68	55.33	49.7	46.22	47.5	46.67	47.67	46.92	47.12	51.52	56.75
TiO$_2$	2.95	2.98	2.91	3.07	3.34	3.3	2.91	3.02	3.47	3.03	3.09	3.07	2.88	2.67	2.65	2.96	3.21
Al$_2$O$_3$	17.24	17.66	16.66	16.86	16.24	16.98	16.78	16.8	18.02	16.93	16.65	17.18	15.99	15.55	15.92	17.07	16.33
Fe$_2$O$_3$	9.26	9.38	8.93	9.41	10.03	9.44	11.55	9.94	10.48	9.5	9.4	9.67	8.99	8.93	9.55	10.18	10.55
MnO	0.15	0.17	0.15	0.27	0.22	0.20	0.13	0.18	0.18	0.18	0.18	0.18	0.17	0.49	0.37	0.32	0.07
MgO	6.74	6.74	6.55	7.42	6.40	6.26	5.30	5.59	5.68	7.96	7.73	7.71	8.02	6.77	7.52	5.46	5.23
CaO	4.59	5.83	5.36	1.72	1.77	1.74	1.62	1.58	4.77	5.88	5.13	4.64	6	6.17	6.57	6.07	1.29
Na$_2$O	4.49	4.21	4.47	4.78	4.89	4.76	6.45	6.45	4.53	4.39	4.49	4.48	4.56	4.66	5.33	4.43	3.13
K$_2$O	2.40	2.57	2.47	2.59	2.50	2.08	2.97	2.94	2.85	2.25	2.11	2.30	1.92	2.51	0.80	2.93	3.38
P$_2$O$_5$	1.62	1.73	1.62	1.60	1.64	1.47	1.93	1.50	1.92	1.43	1.58	1.64	1.63	1.50	1.38	1.71	1.96
LOI	2.79	2.95	3.11	4.55	3.88	3.86	3.08	1.53	4.90	4.23	4.22	4.19	4.23	3.05	5.41	4.08	2.12
Total	101.63	101.89	102.19	102.89	101.98	101.23	101.78	101.12	100.50	102.00	102.08	101.73	102.06	100.02	102.62	100.02	101.32
(ppm)																	
Ti	17700	17880	17460	18420	20040	19800	17460	18120	20820	18180	18540	18420	17280	16020	15900	17760	19260
K	19920	21331	20501	21497	20750	17264	24651	24402	23655	18675	17513	19090	15936	20833	6640	24319	28054
P	7072.92	7553.18	7072.92	6985.60	7160.24	6418.02	8426.38	6549.00	8382.72	6243.38	6898.28	7160.24	7116.58	6549.00	6025.08	7465.86	8557.36
Ba	249	250	245	194	379	340	335	344	351	213	212	203	214	202	195	367	391
Rb	22.84	24.14	23.08	23.16	21.01	21.67	25.43	25.47	22.23	18.91	18.85	19.04	17.14	23.12	12.85	25.79	25.00
Sr	1034	1009	1027	1532	321	318	145	164	1050	1686	1572	1756	1465	800	1540	387	206
Cr	102	110	108	121	bdl	100	97	99	100	116	105	117	124	146	147	100	113
Ni	46	59	47	32	bdl	bdl	bdl	bdl	42	55	52	60	58	37	56	44	35
Cu	414	261	133	137	93	110	210	175	409	124	262	394	517	48	74	151	39
Zn	104	115	102	1725	1174	1296	1003	880	124	128	87	106	85	52	127	330	83
Sc	21.5	19.5	20.15	23.98	13.55	13.96	11.05	11.15	20.48	22.33	20.77	21.04	21.53	20.31	19.53	31.24	17.27
Li	180	131	193	252	175	181	87	67	177	192	212	166	216	300	234	164	275
Nb	23	20	24	20	22	24	23	23	21	18	23	22	21	22	17	22	22
Y	35	29	30	25	50	47	47	47	37	25	35	28	29	38	24	37	45
Zr	272	240	232	220	478	535	405	482	567	258	272	204	286	200	292	415	497
Th	2.10	1.85	1.89	2.40	2.94	3.28	2.94	3.02	2.98	1.86	1.89	1.90	1.75	2.00	2.07	2.98	2.99
La	19.48	19.17	19.14	16.96	35.74	31.29	31.12	31.23	21.44	19.49	19.61	20.13	19.24	25.45	23.35	20.26	43.31
Ce	43.28	41.51	41.47	42.87	81.00	78.79	66.79	64.75	45.35	42.57	43.19	43.71	42.09	55.17	49.60	44.96	94.85
Pr	5.23	5.05	5.06	4.85	9.58	8.27	8.01	7.88	5.59	5.26	5.28	5.37	5.20	6.67	5.96	5.66	10.22
Nd	23.60	22.67	22.76	22.01	41.20	35.79	34.99	34.04	25.26	23.64	24.01	24.38	23.39	30.69	27.14	27.20	42.50
Sm	5.40	5.15	5.14	4.88	8.12	7.94	7.62	7.29	5.76	5.45	5.52	5.59	5.42	6.55	5.74	6.40	7.99
Eu	1.80	1.70	1.72	1.71	1.83	2.03	2.13	2.03	1.92	1.88	1.88	1.91	1.84	1.73	1.57	1.76	2.30
Gd	5.77	5.45	5.50	5.23	9.14	8.10	7.90	7.37	6.07	5.73	5.79	5.88	5.68	7.04	6.19	7.11	7.49
Tb	0.84	0.79	0.80	0.75	1.26	1.15	1.13	1.06	0.89	0.84	0.85	0.86	0.84	0.93	0.82	0.98	0.90
Dy	4.73	4.45	4.55	4.42	6.76	6.47	6.41	5.87	5.05	4.78	4.84	4.92	4.76	6.04	5.24	6.61	5.46
Ho	0.90	0.84	0.86	0.89	1.25	1.23	1.22	1.14	0.95	0.90	0.93	0.94	0.89	1.02	0.89	1.15	0.92
Er	2.47	2.37	2.38	2.67	3.48	3.56	3.47	3.28	2.66	2.55	2.59	2.62	2.48	2.88	2.53	3.24	2.76
Tm	0.47	0.46	0.46	0.38	0.46	0.49	0.47	0.45	0.35	0.34	0.34	0.35	0.33	0.38	0.35	0.43	0.39
Yb	2.90	2.94	2.91	2.54	3.00	3.22	3.07	3.07	3.20	2.17	2.23	2.24	2.15	2.65	2.44	2.96	2.94
Lu	0.35	0.36	0.34	0.34	0.38	0.40	0.39	0.39	0.42	0.30	0.30	0.30	0.29	0.34	0.31	0.36	0.39
AI	50.16	48.11	47.85	60.63	57.20	56.20	50.67	51.51	47.84	49.85	50.57	52.33	48.49	46.15	41.15	44.42	66.08
ASI	1.07	1.00	0.96	1.29	1.24	1.39	1.06	1.07	1.05	0.97	1.01	1.07	0.92	0.83	0.91	0.90	1.43
Nb/Y	0.66	0.69	0.80	0.80	0.44	0.51	0.49	0.49	0.57	0.72	0.66	0.79	0.72	0.58	0.71	0.59	0.49
Zr/Ti	0.02	0.01	0.01	0.01	0.02	0.03	0.02	0.03	0.03	0.01	0.01	0.01	0.02	0.01	0.02	0.02	0.03
Tb/Yb	0.29	0.27	0.28	0.30	0.42	0.36	0.37	0.34	0.28	0.39	0.38	0.38	0.39	0.35	0.34	0.33	0.31
La/Sm	3.61	3.72	3.73	3.47	4.40	3.94	4.09	4.28	3.72	3.58	3.55	3.60	3.55	3.89	4.07	3.17	5.42
Y/Nb	1.52	1.45	1.25	1.25	2.27	1.96	2.04	2.04	1.76	1.39	1.52	1.27	1.38	1.73	1.41	1.68	2.05

4. Petrography

4.1. Pillow-Lavas

Macroscopic examination of the samples collected essentially at the surface (Figure 12), shows that this lava consists of several facies with two poles: The first facies is very rich in fairly large vacuoles (300μm) in the center of the pillow (Figure 13b), and the second facies has very few, if any, vacuoles (towards the edge) (Figure 13a). Between these two poles, all the intermediate facies can be found. The almost continuous variation of the vacuolar facies is probably associated with a progressive degassing of the lava during its placement under water. In this macroscopic description, we will limit ourselves to two facies: (i) A facies practically without vesicles and with very little calcite. It is a greenish rock that can sometimes contain very small vacuoles (100μm), where a fine paste and fine calcite crystals can be observed. With a binocular magnifying glass, we can see that this vacuolar calcite is crowned by greenish minerals probably corresponding to chlorites and metallic minerals. This facies can sometimes be rich in metallic minerals, either around the vacuolar calcite, or in fine disseminations in the vitreous paste or in fractures, and (ii) a facies very rich in

vacuoles of varying sizes. The vacuoles are most often filled with late calcite. The relative proportion of vacuoles and their size varies from one outcrop to another and within the same outcrop.

Microscopically, only microlites (80–95%), and more rarely phenocrysts, plagioclases and pyroxenes (augite) are recognizable in a vitreous matrix devoid of recognizable olivines and amphiboles (Figure 13c,d). Plagioclases in microlites sometimes show a mineral linearization materializing schistosity planes (Figure 13e). The other minerals are all of secondary origin related to alterations, such as calcite found either in vacuoles or in the interstices of plagioclases or in late fractures (Figure 13f). Chlorite is associated either with vesicular calcite or in filling schistosity planes. Incidentally, we note the presence of opaque minerals associated either with vacuolar calcites (the facies most rich in calcite contain the highest proportions of these minerals), or disseminated in the rock or in the interstices of plagioclases.
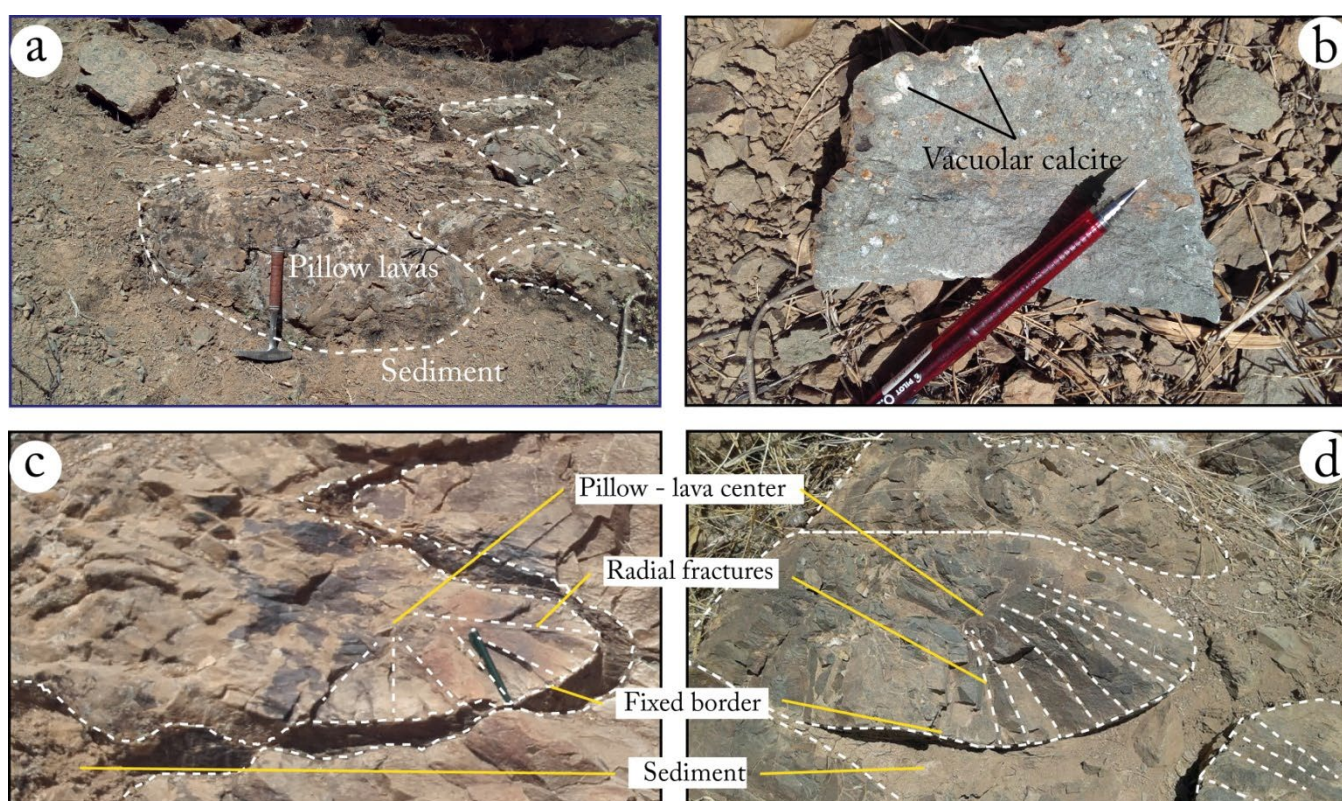
Figure 12. (**a**) Pillow-lavas outcrop, (**b**) vacuolar lava facies, (**c**) detailed pillow structure showing radial fractures and (**d**) pillow in contact with greenish pelites.

4.2. Dolerites

It is a greenish-grey rock with a microgranular texture, in which small blackish and whitish to greyish-whitecrysts can be identified in a greenish matrix (Figures 14 and 15a). A microscopic study of this facies shows a typical dolerite structure. Mesostasis contains rod-shaped plagioclase crysts, more or less sericitized, associated with interstitial pyroxenes, partially or wholly amphibolitized, chloritized tourmaline, rutile and opaque minerals (Figure 15b–h). The latter correspond either to cubic pyrite minerals or to lamellar automorphic minerals (ilmenite and hematite). These opaque minerals are in relatively abundant proportions. It should be noted that this dolerite facies is often altered, as evidenced by the transformation of sericite, chlorite, and calcite plagioclases and pyroxenes into amphiboles (uralitization).
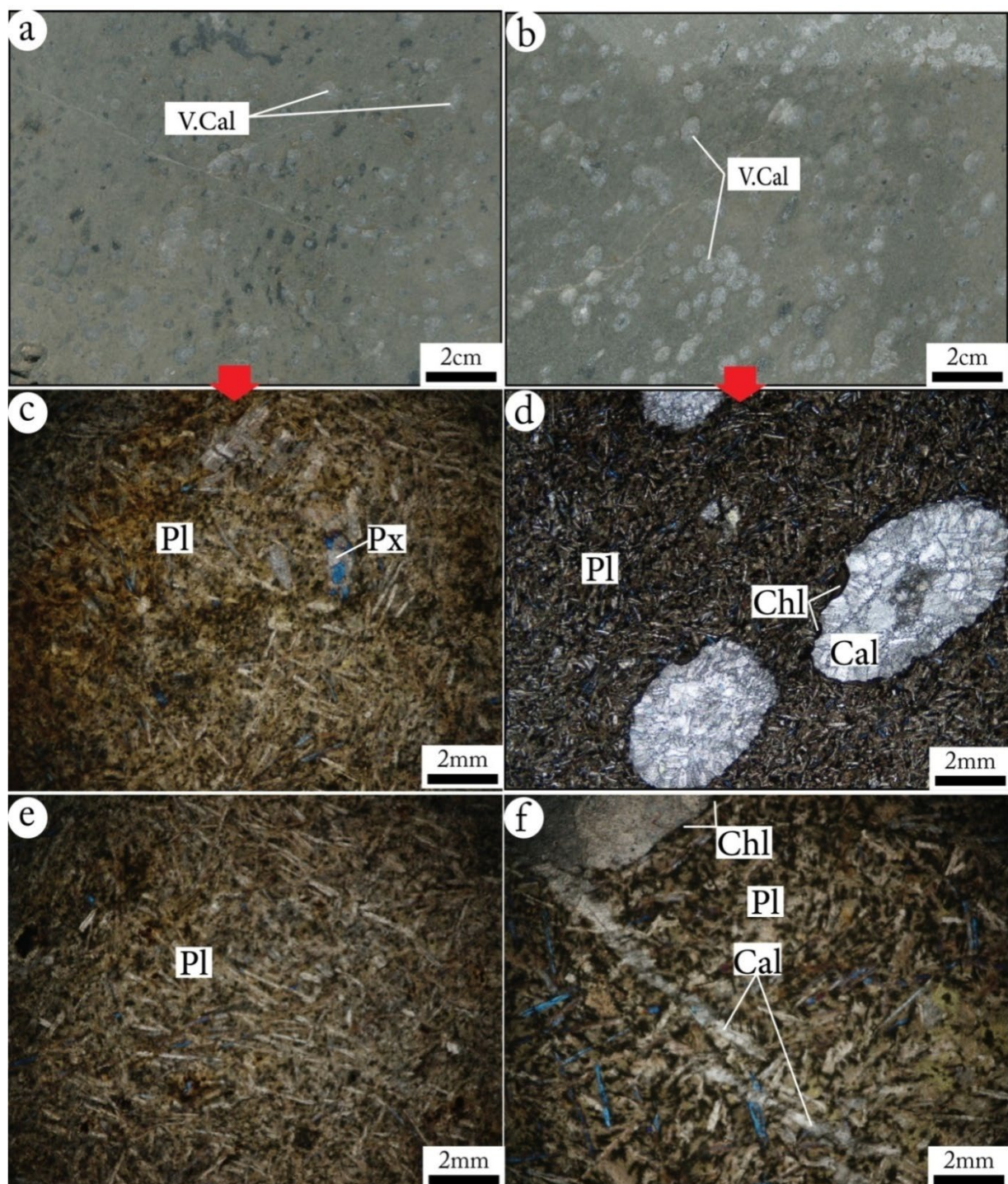
Figure 13. Macroscopic view ofpillow-lavas less (**a**) and rich (**b**) in calcitic vacuoles, and micropho-tographs of this facies in transmitted light with crossed nocols (**c**–**f**). V.Cal: vacuolar calcite, Pls: plagioclase, Cal: calcite, Chl: chloriteandPxs: pyroxene.
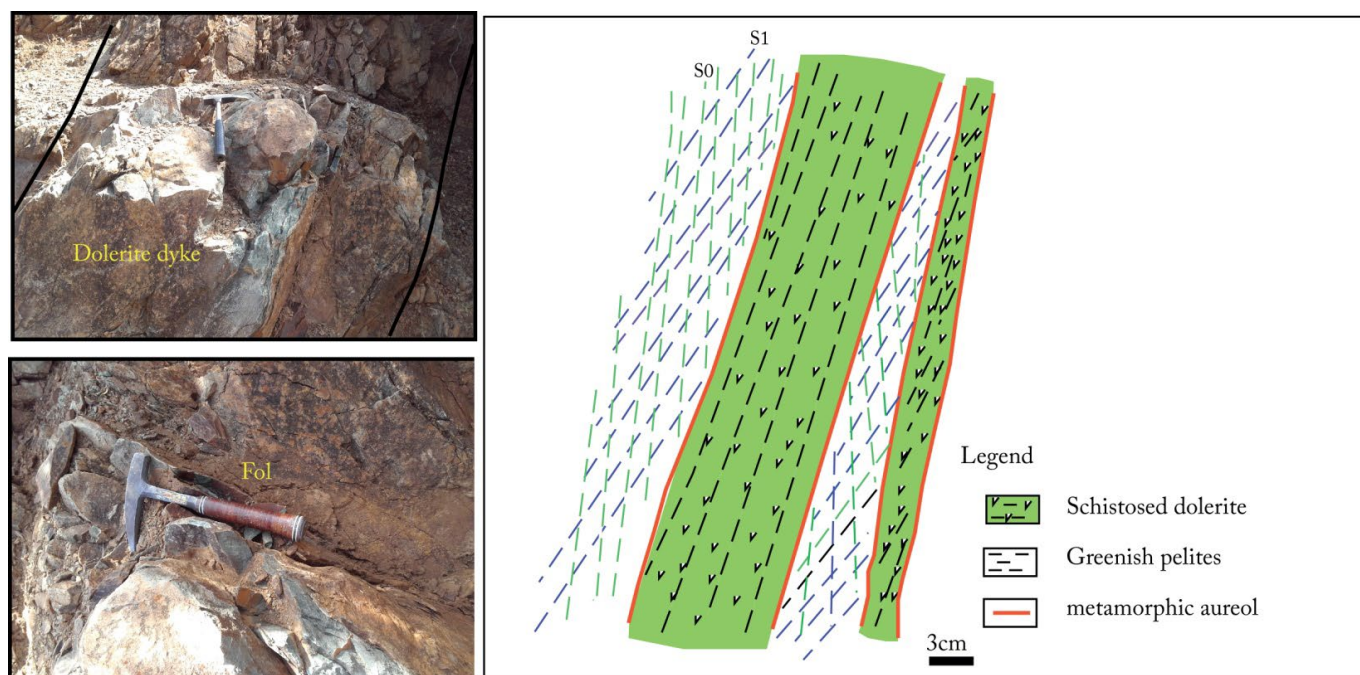
Figure 14. Foliation (Fol) in outcropping dolerites.

4.3. Olivine-Bearing Gabbros

This is a light green rock with abundance of leucocratic elements. It features a coarse-grained texture in which small black and white crysts can be identified in a greenish matrix (Figure 16a). The rock is totally crystallized and shows a grained texture. Mineralogically, it is composed of plagioclases, pyroxenes, olivines, titanites, rutile, tourmaline, apatite and opaque minerals (Figure 16b–g). All cardinal minerals of this rock have undergone a more or less important alteration. Plagioclases are sericitized, albitized, amphibolitized and epidotized, whereas pyroxenes and olivines are serpentinized and chloritized (Figure 17a–h).

4.4. Spilitization

The petro-mineralogical study shows that each of the three magmatic facies in the NNE Achemmach have undergone hydrothermal alteration to a greater or lesser extent. This is well marked on pillow-lavas, which are transformed into true spilites by the albitisation and carbonation of plagioclases, and by the development of chlorites, especially at the level of calcitic vacuoles.

This spilitization has also affected olivine-bearinggabbros, whose plagioclases are sericitized and albitized, amphibolitized and epidotized pyroxenes and serpentinized and chloritized olivines, and to a lesser extent, dolerites, whose plagioclases are more or less sericitized and interstitial pyroxenes are partially or wholly amphibolitized.

The alteration of the cardinal minerals of these three basic magmatic facies: albitization, sericitization and carbonation of plagioclases, amphibolitization (actinote), epidotisation of pyroxenes and chloritization and serpentinization of olivines, associated with a remarkable richness in titanium (abundance of titanite), reflect the effect of an oceanic hydrothermal metamorphism of the green shale type.
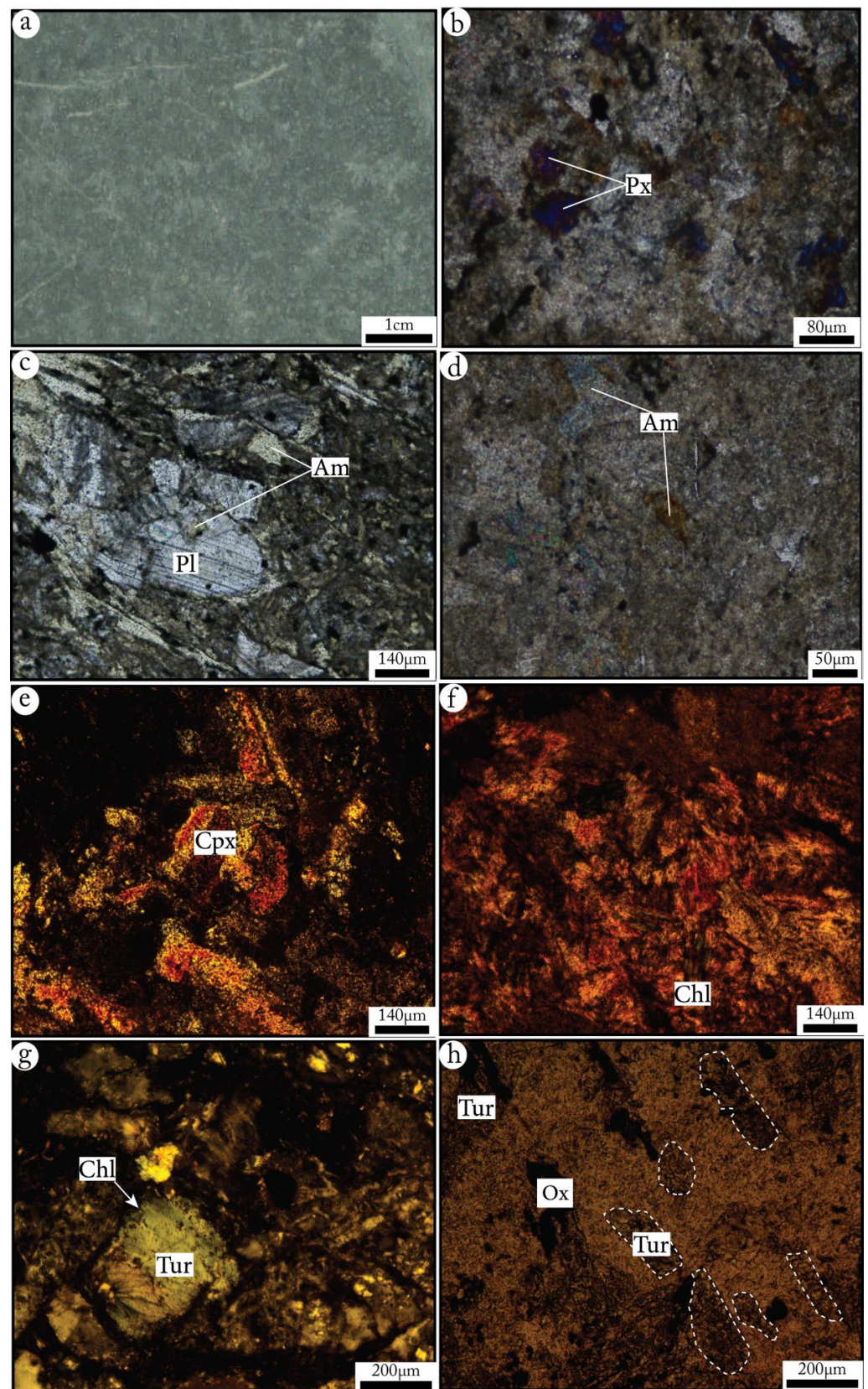
Figure 15. (**a**) Macroscopic view of a dolerite facies. (**b**–**h**) Microphotographs of dolerites: plagioclases (Pl), amphibolitized (Am) pyroxenes (Px), clinopyroxenes (Cpx), chloritized (Chl), tourmaline (Tur) and oxides (Ox) (transmitted light—crossed nicols).
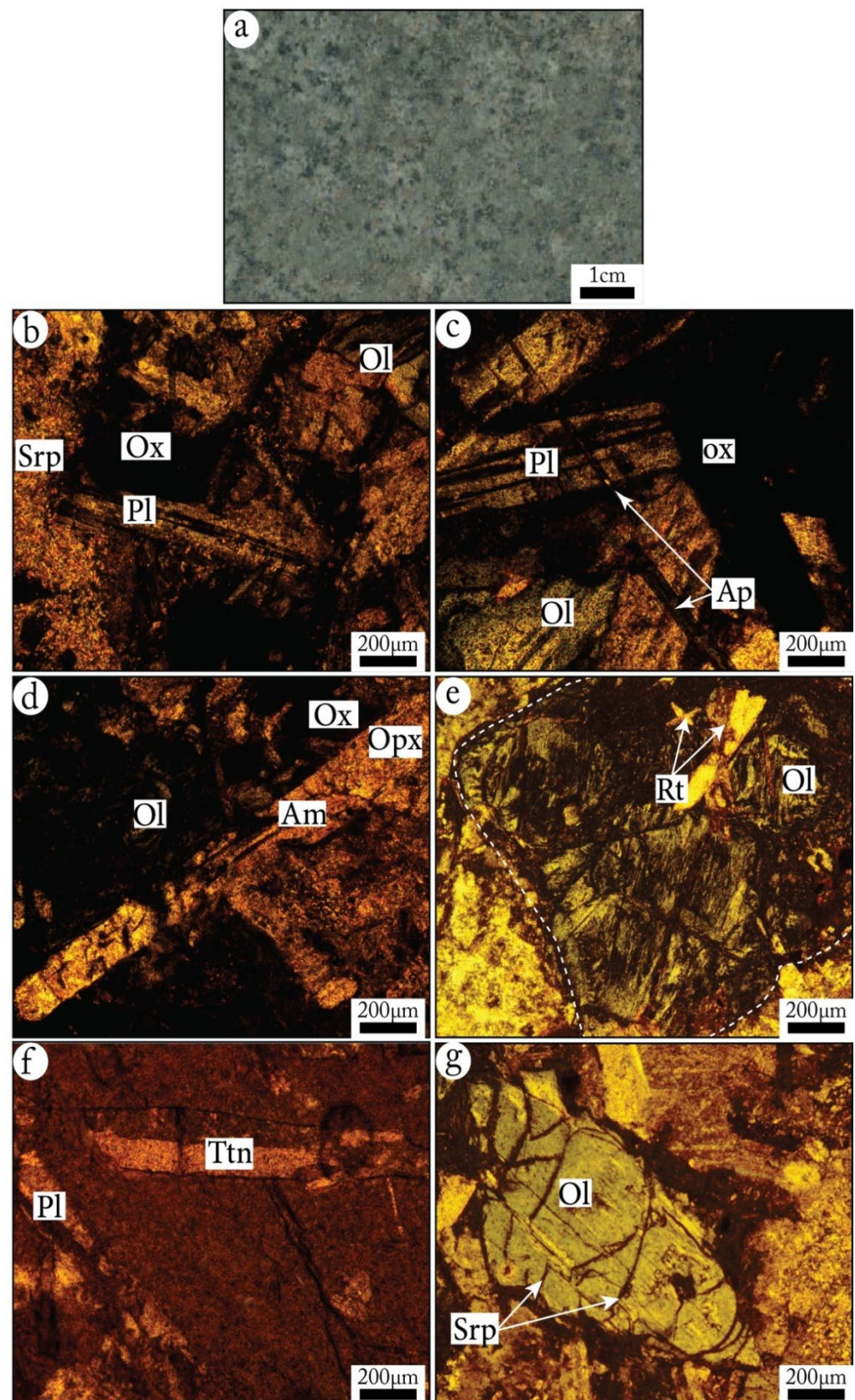
Figure 16. Samples of olivine-bearing gabbros. (**a**) Macroscopic view and (**b**–**g**) microphotographs of olivine-bearing gabbro (transmitted light—crossed nicols). Sericitized (Ser) plagioclases (Pl), amphibole (Am), orthopyroxene (Opx), serpentinized (Srp) olivine (Ol), Titanite (Ttn), apatite (Ap), rutile (Rt) and oxides (Ox) (transmitted light—crossed nicols).
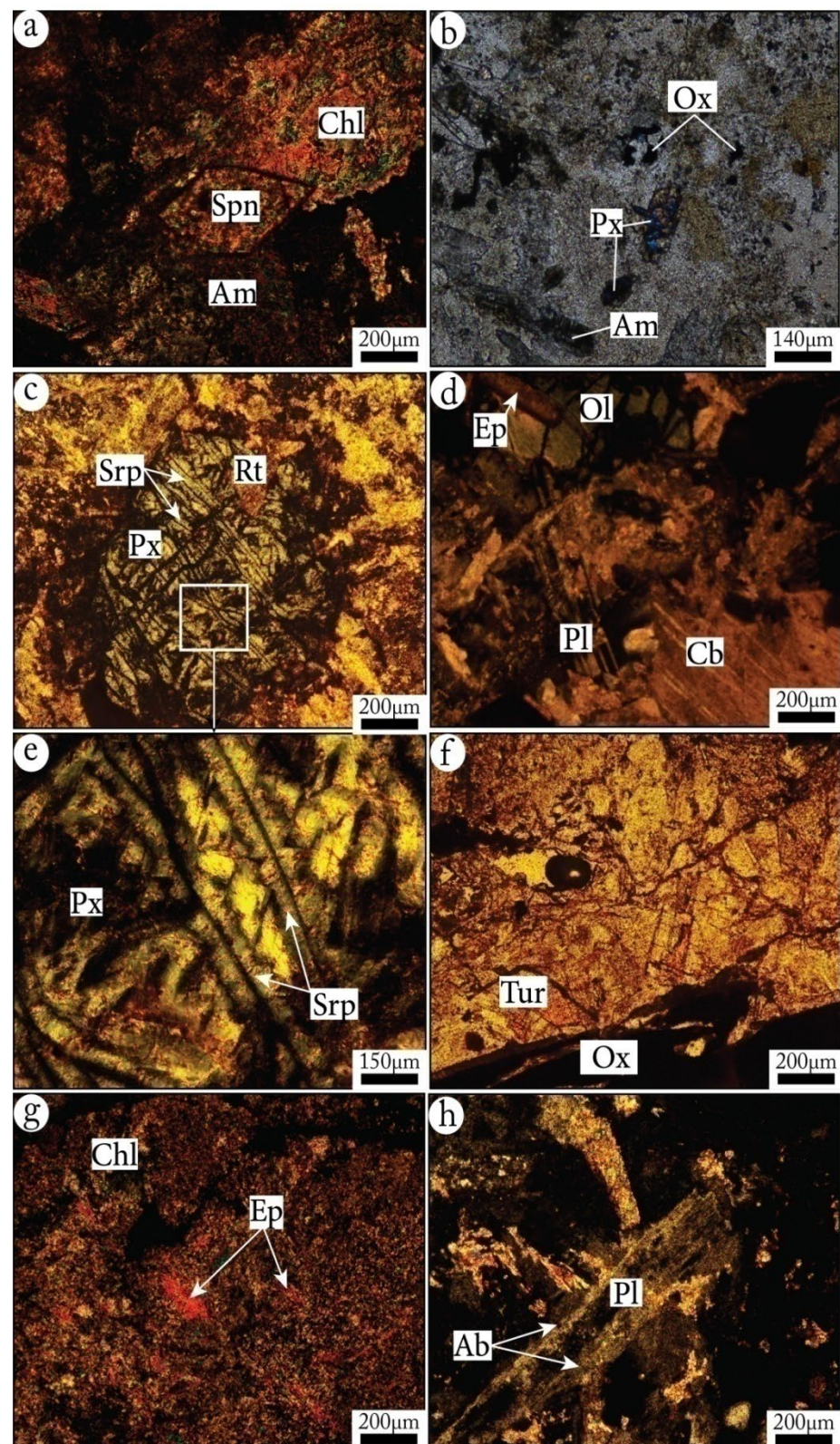
Figure 17. (**a–h**) Microphotographs of the alteration phases of olivine-bearing gabbros: sericitized (Ser) and albitized (Ab) plagioclase (Pl), amphibolitized (Am) and epidotized (Ep) pyroxene (Px), serpentinized (Srp) and chloritized (Chl) olivine (Ol), tourmaline (Tur), and oxides (Ox) (transmitted light—crossed nicols).

5. Geochemical Variations and Typology of Magmas

5.1. Elements' Mobility

The commonly used method for the classification of volcanic and sub-volcanic rocks is the total alkali-silica diagram (TAS) [57]. However, this diagram is not reliable in the classification of altered rocks. Other classification diagrams, based on the consideration of other major elements such as TiO_2, P_2O_5, and Al_2O_3, which may be exceptionally mobile during alteration, fail in the case of the classification of altered rocks and may give misleading results. For these reasons, the use of trace elements has been adopted, which appear to be less sensitive to these alteration processes

The most commonly used approach is the Zr/TiO_2 vs. Nb/Y diagram [58,59], where Nb/Y gives alkalinity (Na_2O+K_2O) and Zr/TiO_2 gives silica. The Nb/Y ratio increases from sub-alkaline to alkaline compositions, while the Zr/TiO_2 ratio decreases from acidic to basic compositions. For classification purposes, the mobility of all selected elements must be evaluated. An effective method is that of [60], in which the mobility of an element is tested using variation diagrams. If the two elements are moderately to highly incompatible and immobile, and the samples are co-genetic, the data should show correlations with slopes close to unity. For this study, Nb is the element used, as it is one of the most immobile elements.

The behavior of major and some trace elements with respect to Nb is illustrated by the binary correlation diagrams in Figure 18.

5.2. Major Elements

The diagrams in Figure 18 show scattered point clouds covering a wide range of chemical composition of these rocks. It probably reflects the effect of alterations that have affected these rocks and have an effect on the mobility of many elements, mainly: Si, Na, K, Ca, Mg and Al, and to a very small extent, Ti. Thus, when these samples are plotted in the SiO_2 vs. Nb/Y diagram, they show a wide variation in SiO_2 contents, indicating that the silica was mobile during the hydrothermal processes. The effects of such processes are most apparent when the samples are plotted in the TAS [57,61]; R1–R2 [62] diagrams (Figures 19 and 20).

The R1-R2 diagram [62] classifies magmatic rocks according to their cationic proportions through the study of all the major chemical elements in the rock. In addition, it seems that among the three identified groups of rocks, plutonic rocks (olivine-bearing gabbros) are the least affected by alteration processes. The fact that all samples were affected by post-magmatic alteration is also confirmed by the peraluminous character (Figure 19b) that marks many of them, and which is expressed by high values of the alumina saturation index.

5.3. Trace Elements

With respect to Nb contents, two families of rocks can be distinguished (Figure 16): rocks with low Nb content (Tables 1–3), and others with high Nb content. With the exception of P_2O_5, TiO_2 and, to a lesser extent, SiO_2, the low Nb samples are widely dispersed and show no correlation. Contrarily, samples with high Nb content are more correlated.

The behaviors of Zr, Ti and Y are totally different. The three rock types (pillow-lavas, olivine-bearing gabbros and dolerites) can be identified (Figure 18, Tables 1–3). In each type of rocks, the elements Zr, Ti and Y vary proportionally to Nb (positive correlation). The observed dispersion could be related to disturbances due to hydrothermal leaching. However, although affected by weathering, these elements are still the most appropriate for classification. Their relationship during magmatic differentiation and hydrothermal weathering remains almost unchanged.
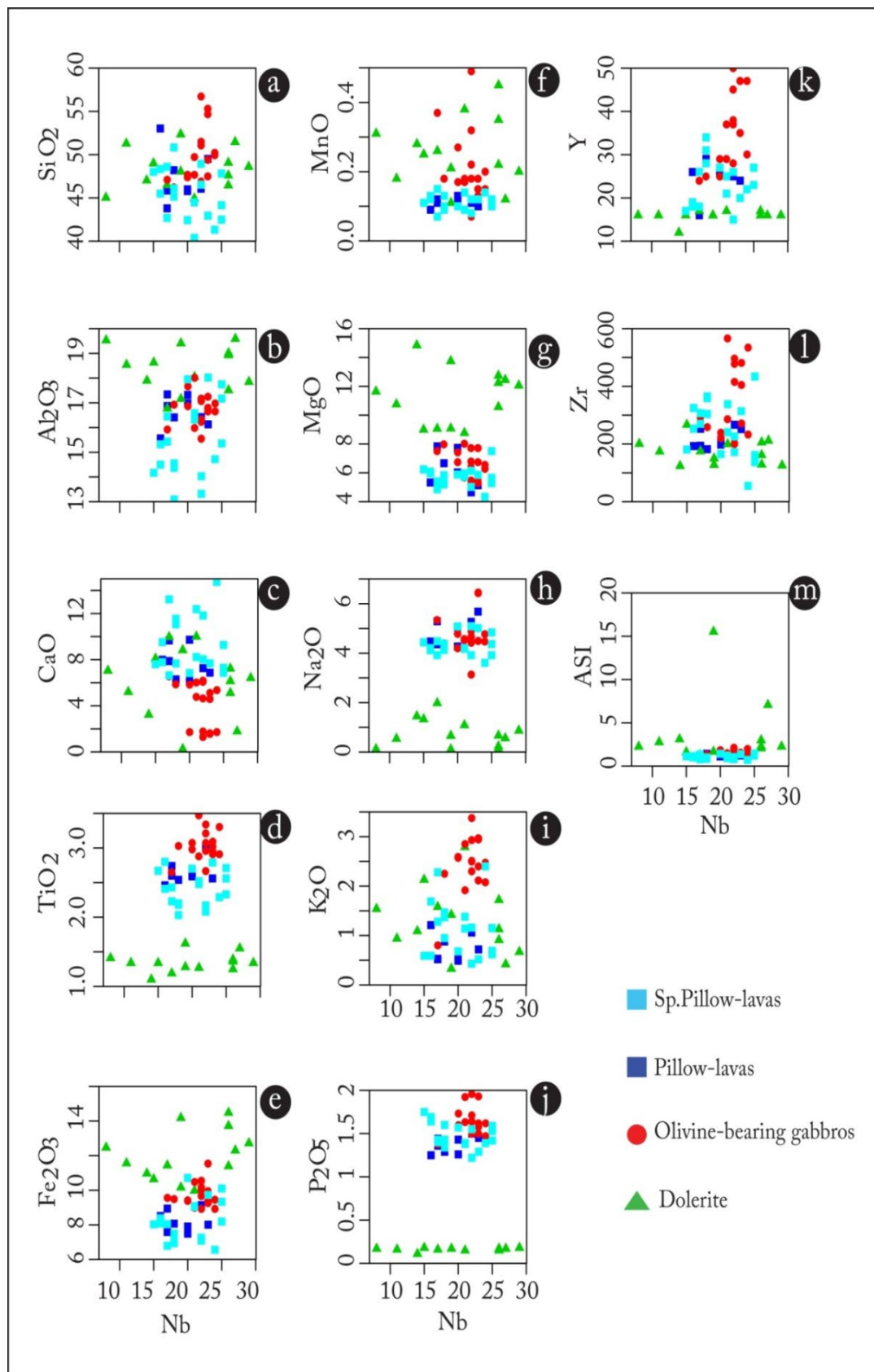
Figure 18. Variations of selected major (wt%) (**a–j**), trace element (ppm) (**k,l**) and Alumina Saturation Index: ASI = Al/(Ca + Na + K) molar (**m**) contents vs. Nb (ppm) for the mafic and intermediate dikes in the NNE Achemmach.
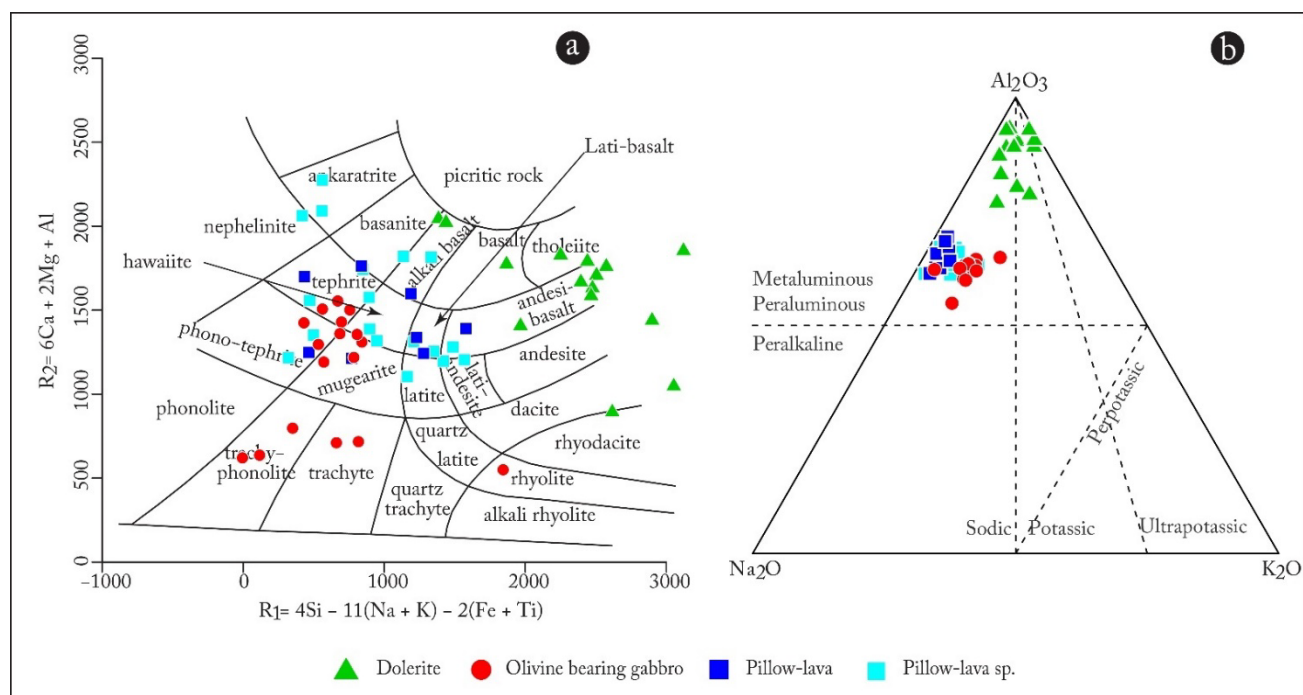
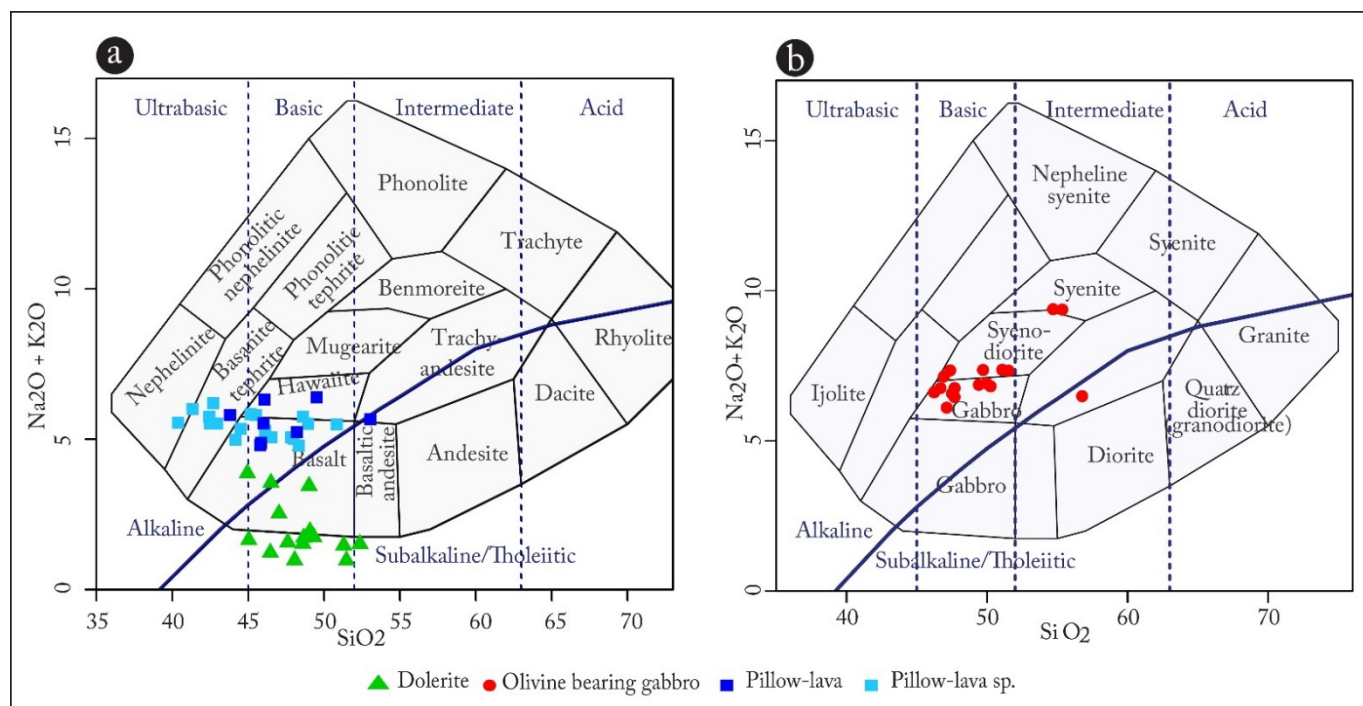**Figure 19.** (**a**) R1-R2 [62] and (**b**) Na_2O-Al_2O_3-K_2O (molar) diagrams [63].

Figure 20. (**a**) SiO_2-Na_2O+K_2O [57] "Volcanic rocks", and (**b**) SiO_2-Na_2O+K_2O [57] "Plutonic rocks" diagrams.

5.4. Classification

The rocks in the NNE Achemmach area have undergone advanced hydrothermal alteration and a consequent leaching of the major elements (Si, Na, K, etc.). Therefore, the classification of these rocks has been conducted considering immobile or slightly mobile elements, and different discrimination diagrams have been used to discuss the geochemical

signatures of these rocks. Thus, in the Zr/TiO$_2$ vs. Nb/Y diagram (Figure 19), samples from three facies (pillow-lavas, olivine-bearing gabbros and dolerites) are clearly reported in the field of alkaline basalts with a high Nb/Y ratio (Figure 21a,b).

5.5. Magmatic Affinity and Geodynamic Significance

5.5.1. Pillow-Lavas

All the analyzed rocks demonstrate an alkaline affinity indicated by the values of the Nb/Y ratios and the high TiO$_2$ and P$_2$O$_5$ contents. In the diagram of Figure 21, they are shown in the alkaline basalt field. The positive Nb anomalies in the normalized to the original mantle diagram (Figure 24) give evidence of the alkaline character of these rocks.

In the MORB (Mid Ocean Ridge Basalt) normalized diagram (Figure 22), pillow-lavas show profiles of the Oceanic Island Basalt (OIB) type, characterized by high and moderate enrichments in LILE (Large Ion Lithophilic Elements) and HFSE (High Field Strength Elements), respectively, and negative K and Zr anomalies. As with olivine-bearing gabbros, the wide variation in LILE is likely to represent the result of the alteration.

The close similarity between these rocks and the alkaline magmas can also be observed in the normalized diagrams to the original mantle, where high concentrations of LILE and HFSE associated with positive Nb and negative K anomalies support the anorogenic nature of the original magmas. This suggests that crustal contamination did not play a significant role in their petrogenesis.

Moreover, the comparison between Th/Yb and Ta/Yb ratios shows that these rocks are in the mantle domain, which confirms a weak involvement of the crustal component. The REEs are fractionated (Figure 23), so the REE spectra normalized to chondrites indicate a mantle source with the probable presence of garnet. The enrichment in LREELight Rare Earth Elements) shows that the character of the enriched mantle source is not due to crustal contamination from subduction processes.

5.5.2. Olivine-Bearing Gabbros

In the Zr/TiO$_2$ vs. Nb/Y diagram (Figure 21), and with the exception of two samples that are reported in the trachy-andesite field, all rocks analyzed demonstrate an alkaline affinity, as indicated by the high Nb/Y ratio values. Standardized plots with respect to the original mantle (PM) and MORB (Figures 22 and 24) reveal trends that essentially resemble those of pillow-lavas (enrichment in LREE and HFSE, positive peak in Nb, enrichment in HREE, negative Ti and P anomalies and positive peak in Zr). These similarities also appear in the diagram of Figure 23, where the LREE have highly fractional profiles similar to those of dolerites, while the HREE are flat and resemble pillow-lavas' profiles. Some variations of these diagrams in Figure 25b,c support co-genetic links between olivine-bearing gabbros and pillow-lavas. In this case, the olivine-bearing gabbros would have been derived from the same magma producing pillow-lavas, and the dolerites would have been their evolved product. Indeed, the decrease in the quantity of ferromagnesian minerals and the increase in plagioclases are in line with this evolution.

The strong affinities with dolerite samples can be explained as the result of assimilation or interaction with pillow-lava-like material during magmatic evolution.
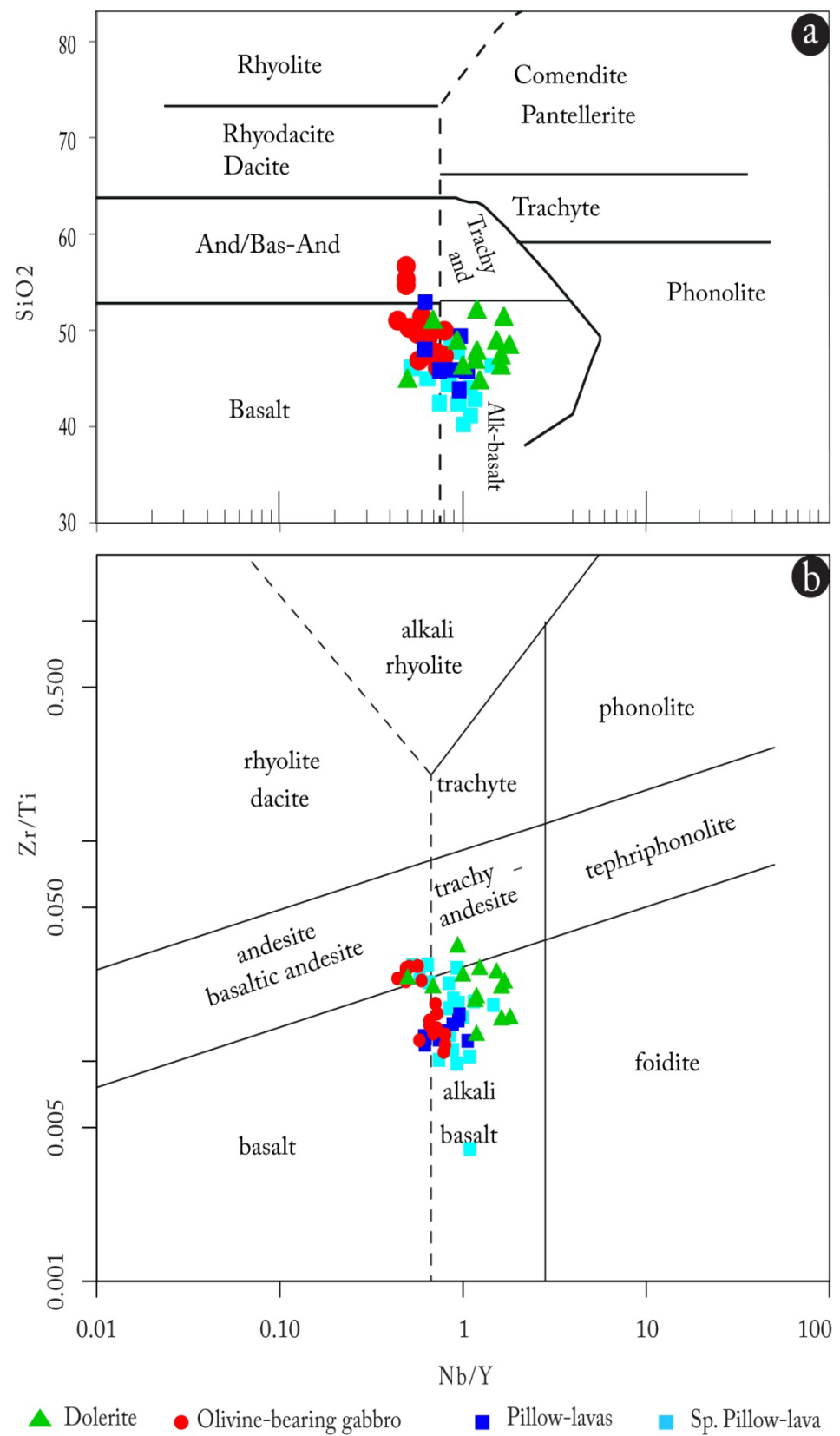
Figure 21. (**a**) Zr/TiO₂ vs. Nb/Y and [59] (**b**) SiO2 vs. Nb/Y [58] diagrams. Dotted lines: boundary between the sub-alkaline (on the left) and alkali (on the right) fields.
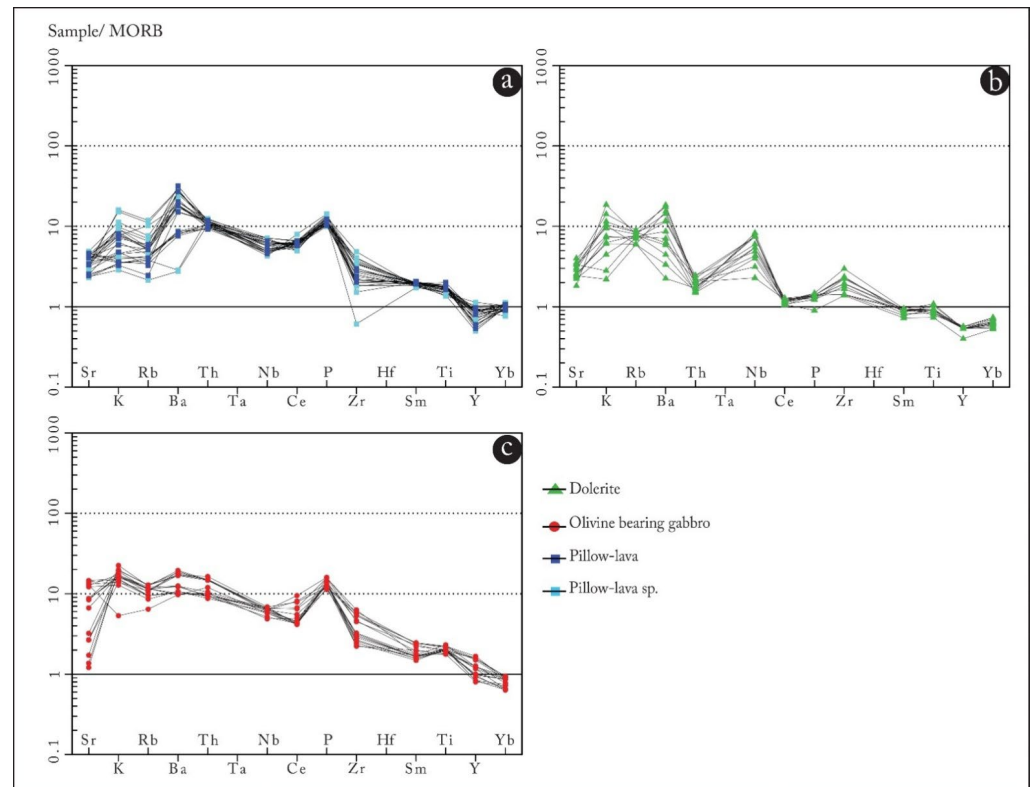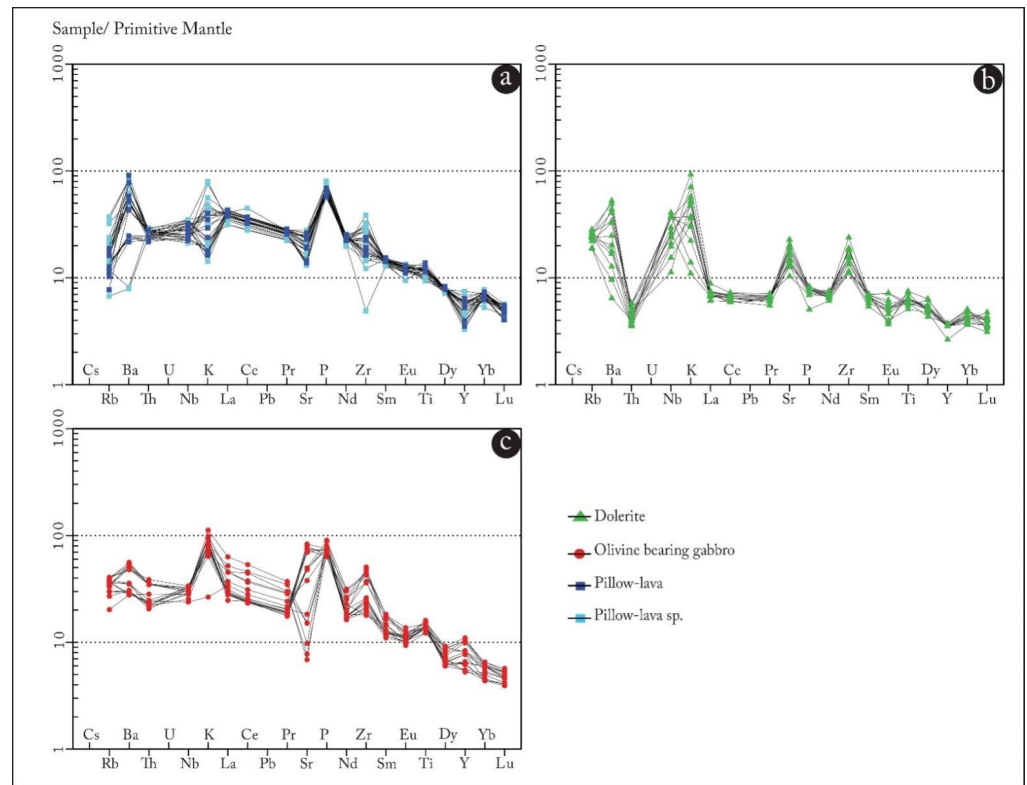
Figure 22. Multielement diagrams normalized to MORB [64] or magmatic rocks of NNE Achemmach. (**a**): Pillow-lavas, (**b**): dolerites, (**c**): Olivine-bearing gabbros.
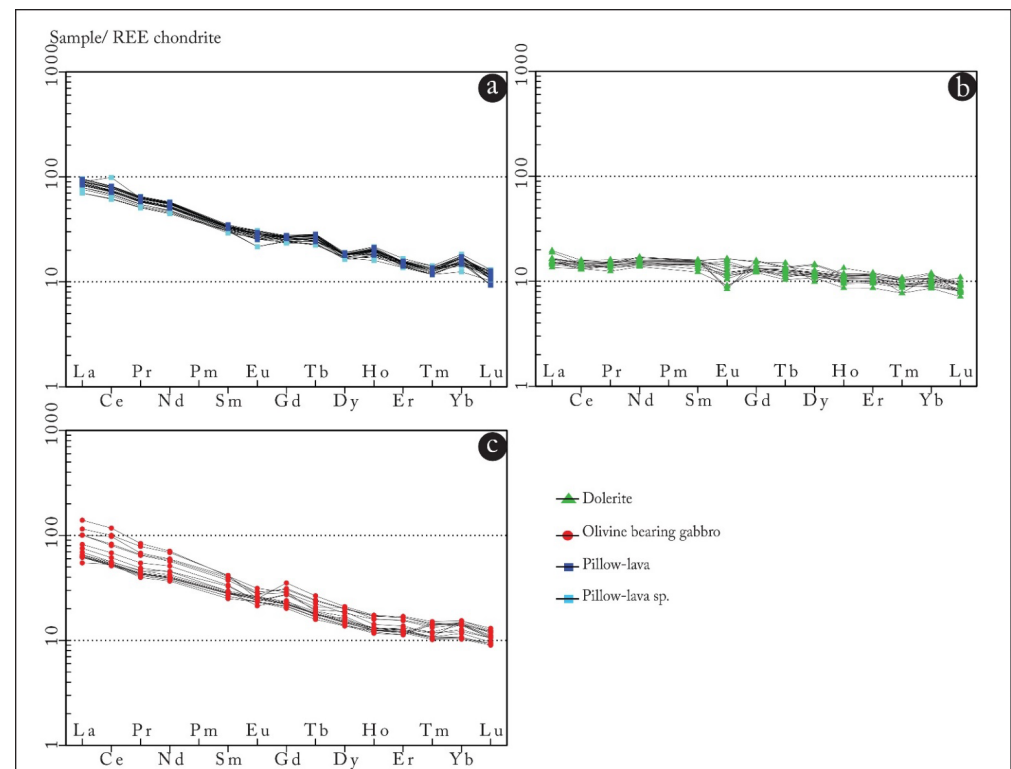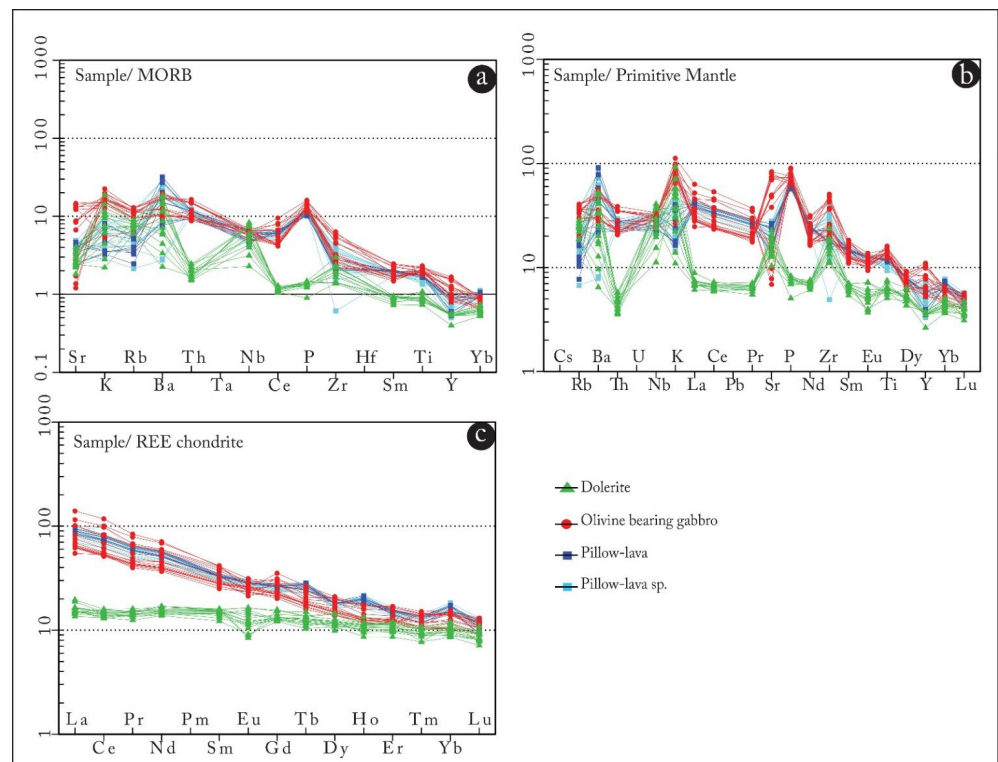

Figure 23. Spectra of rare earths normalized to chondrites [65] for magmatic rocks ofNNEAchemmach. (**a**): Pillow-lavas, (**b**): dolerites, (**c**): Olivine-bearing gabbros.

Figure 24. Multielement diagrams normalized to primitive mantle [66] for magmatic rocks of NNE Achemmach. (**a**): Pillow-lavas, (**b**): dolerites, (**c**): Olivine-bearing gabbros.

Figure 25. Multielement diagrams normalized to MORB [64] and (**a**) to primitive mantle [66] (**b**), spectra of rare earths normalized to chondrites [65] and (**c**) for magmatic rocks in the NNE Achemmach.

5.5.3. Dolerites

In the Zr/TiO$_2$ vs. Nb/Y diagram (Figure 19), all samples are grouped in the alkali basalt field. The fractionation of minerals (Figure 21b) results from fractional crystallization and displacement of magma. This indicates that these rocks do not represent magmas from which they would have crystallized. Nevertheless, when normalized to the prime mantle (PM) [66] (Figure 24b), the samples demonstrate patterns comparable to those of magmas related to subduction, demonstrating a general enrichment in LILE and HFSE. Still, the weak positive Nb anomaly suggests alteration effects or alkaline affinity. This feature has been reported in the eastern part of the Fourhal Basin in gabbroic veins, associated dolerites and basaltic flows [67].

6. Discussion

The geodynamic context of the intrusions of the Moroccan Central Hercynian Massif is complex, particularly because of the rate of alteration, the scarcity of outcrops and the studies carried out thus far. Some interpretations concerning their affinity and their emplacement conditions are even contradictory [4,8,36,67,68].

Notwithstanding the complexity of defining the geotectonic context of the Achemmach NNE dikes from the literature, the succession of magmatic-hydrothermal events and the chemical evolution of the dikes will be discussed and interpreted in comparison with known geodynamic scenarios in the Hercynian chain at the end of the Permian.

Preliminary studies carried out mainly by [4,5], distinguished, with reference to the major deformation phase, two magmatic provinces: (i) the Eastern Meseta province, marked by post-orogenic volcanism with a calco-alkaline geochemical signature dated to the Upper Visean and (ii) the Western Meseta province, whose basic magmatism is defined as prior to the Variscan orogeny. This province is underlined by underwater effluxes and intrusions of sub-Visean age at Namuro-Westphalian. Other researchers suggest a different scenario. According to [69], the magmatic intrusions of the Eastern Jebilet and Azrou-Khenifra basins are subsequently affected by post-Visian Hercynian tectono-metamorphic events. They present chemical characters of alkaline magmatic series set up in an anorogenic intracontinental context. For [3,5,6], the basic magmatism of the central Jebilet is syntectonic, set up during the synschist regional deformation.

These interpretations have been questioned by a number of scholars [7–9,67], based on several integrated tectono-sedimentary and magmatic studies. For these authors, the mafic magmatic bodies within the carboniferous series were emplaced in the context of an upper plate foreland basin accompanying a deformation continuum beginning early in the east and propagating as the collision progressed westward through arcuateorogenic fronts.

More recently, [10] identified a new effusive and explosive volcanic activity (Visean-Serpukhovian) in the western part of the Meseta, which varies in nature from basalts to rhyolites and assumes a similarity to the volcanic activities recognized in the eastern area.

Concerning the magmatic formations in the NNE of Achemmach area, this study allows one to distinguish two groups of rocks with different chemical characteristics: alkaline pillow-lavas and olivine-bearing gabbros, on the one hand, and dolerites, which show both an alkaline to tholeiitic signature, on the other hand, and which can be related to basalts of the transitional alkaline series (Figure 23b) [69]. The relationships between these rocks are not very obvious; however, a chemical evolution appears between these two groups (Figure 18f,j,k,h). Moreover, the spectra of the multi-element diagrams as well as those of the rare earths (Figures 21–24) show the same evolution between the groups of each set.

On a geodynamic level, according to the diagrams of [70–72] in Figure 26, the rocks in the NNE sector of Achemmach are located in the intraplate basalt field.

According to the petrological and geochemical studies carried out in this work and the data from the Meseta literature, the sequence of magmatic events in the NNE sector of Achemmach would be presented as follows:

The first magmatic event would be syn-orogenic. It is manifested by basic rocks of alkali-tholeiitic character (dolerites) and by acid rocks represented by known rhyolites in the El Hammam sector. The rhyolites and microgranites will thus be the last to be put in place before the granite since they have suffered the consequences of the boron post-magmatic circulations (boron post-magmatic circulations), which is obvious in El Hammam [11,31,32,73].
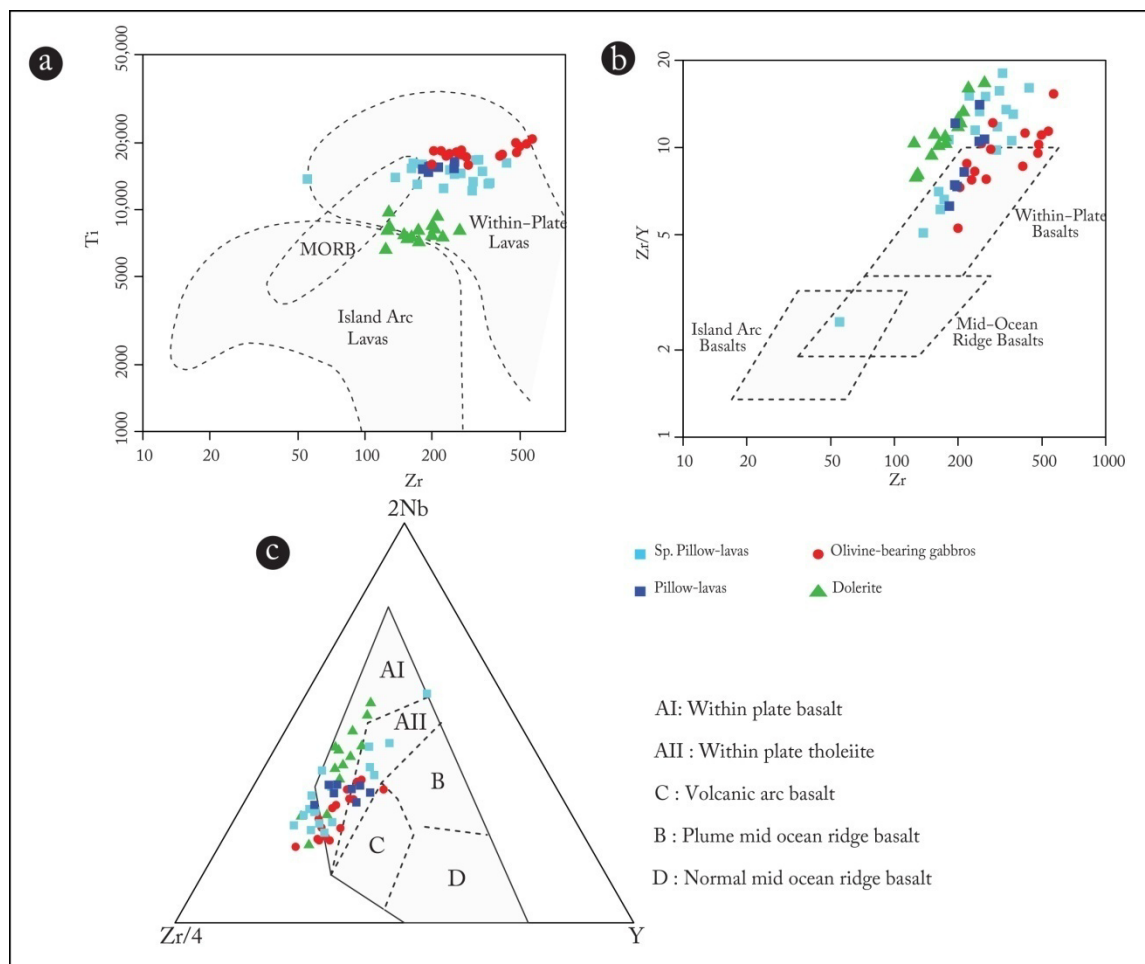
Figure 26. Zr-Ti [71] (**a**), Zr-Zr/Y [70] (**b**) and Zr/4-2Nb-Y [72] (**c**) diagrams.

The second magmatic event is syn- to late-orogenic (Figure 27). It would correspond to the introduction of pillow-lavas with a basic impression (Figure 21b). These would be comparable to the folded and fractured rocks of Mrirt with alkaline affinity described by [33,67] and the basalts of Tazzeka, studied by [4]. These alkaline rocks are interstratified in the Upper Visean series and constitute the first magmatic event followed by the formation of the Serpukhouvian sills and calcareous basalts. These rocks are considered syn-orogenic since they are associated with the opening and filling of orogenic carboniferous basins. The apparent alkalinity of some of these rocks has been widely discussed in the work of [67]. These rocks are thought to be related to the evolution of mafic magmas during their ascent and emplacement in the carboniferous basins, as well as the weak Paleozoic formations that overhang them during this period.

The third magmatic event is post-orogenic (Figure 27). It is represented by transition rocks where there is a coexistence between a previous orogenic and anorogenic magmas. This late magmatic event has an alkaline affinity and corresponds to olivine-bearing gabbros.
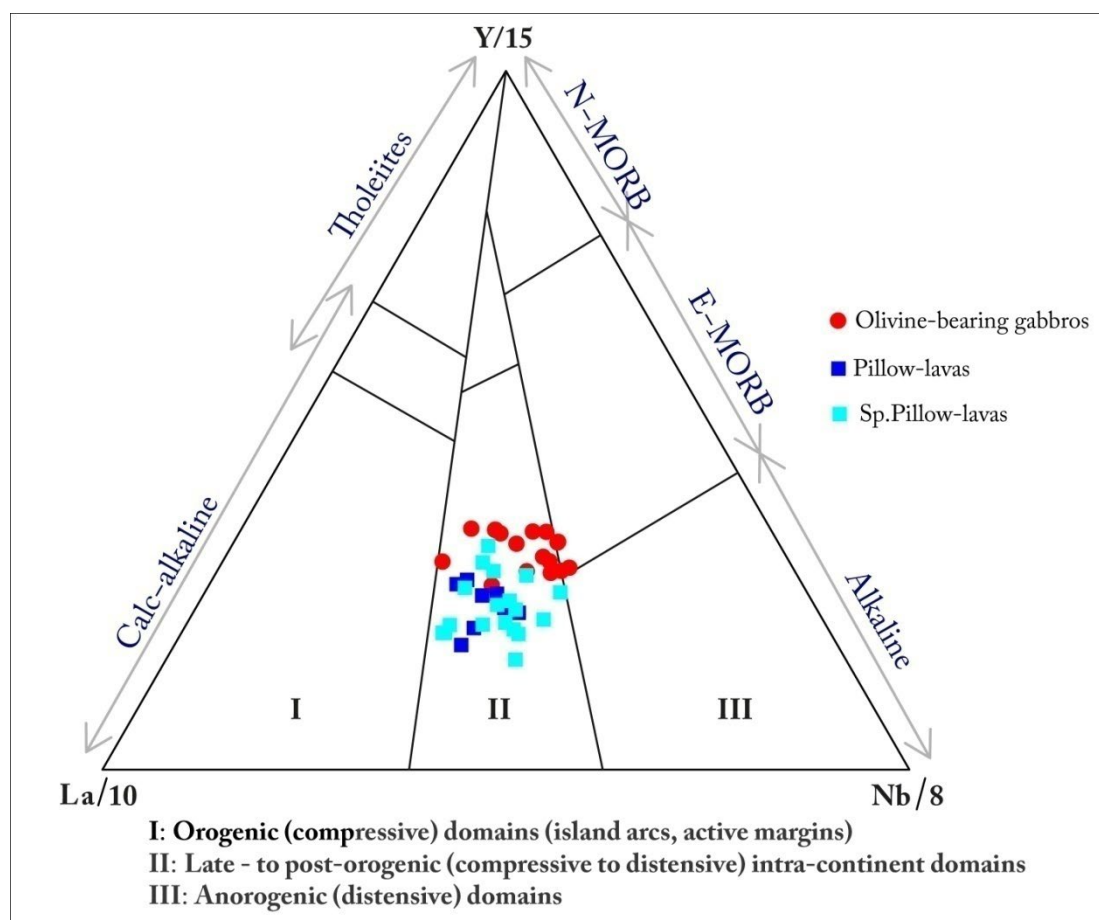
Figure 27. La vs. Y vs. Nb ternary classification diagram [74].

7. Conclusions

The NNE Achemmach sector is made up of two main units: limestones and sandstone shales, of Middle to Upper Visean age for the first unit, and flyschs of Upper Visean-Namurian age for the second one. These two formations demonstrate anomalous contact materialized by a shear zone of a NE-SW to NNE-SSW direction.

Structurally, the formations of this sector demonstrate an evolution comparable to those of the terrains of El Hammam district and those of the Agourai region. The structures are: (i) A major structure in NE-SW to NNE-SSW of synschist folding, linked to the main phase of the Hercynian orogeny under an epizonal metamorphic climate, (ii) an important early volcanic and hypovolcanic magmatic activity at the major deformation, (iii) some shear zones of regional extent that would have been straddling before shearing, showing a northward shift in direction and marking a major structure vergeand (iv) NE-SW to NNE-SSW faults subparallel to the schistosity and N130 to N150 faults with sinister play, having affected all previous structures.

The emplacement of the magmatic rocks in this region would have started with dolerites during the major Hercynian phase (NW-SE shortening), followed by basic pillow-lavas with traces of ductile shear and, finally, that of the olivine-bearinggabbros, whose outcrops are not schistose.

Compared to the known magmatic rocks at the scale of the El Hammam-Achemmach district and the Massif Central, and taking into account their textural and petrological characteristics, dolerites would be syn-tectonic and pillow-lavas and olivine-bearing gabbros would be syn- to late-tectonic.

Pillow-lavas and olivine-bearing gabbros have an alkaline affinity, while dolerites have a transitional alkaline affinity (alkali-tholeitic).

These magmatic formations would thus have been established in an anorogenic intra-continental geodynamic context corresponding to a basin magmatism in a poorly evolved opening, having undergone an oceanic alteration at the origin of the spilitization that develops there.

References

1. Michard, A. *Éléments de Géologie Marocaine*; Éditions du Service Géologique du Maroc: Rabat, Morocco, 1976.
2. Fadli, D. Evolution Sédimentaire et Structurale Des Massifs Des Mdakra et Du Khaouat; Deux Segments Hercyniens de La Meseta Marocaine Nord-Occidentale. Bachelor's Thesis, University of Rabat, Rabat, Morocco, 1990; 316p.
3. Essaifi, A. Le Magmatisme Acide-Basique Des Jbilet Centrales. Ses Relations Avec La Déformation Hercynienne Synschisteuse. Implications Géodynamiques. Master's Thesis, Caddi Ayyad University, Marrakech, Morocco, 1989.
4. Kharbouch, F. Les Laves Dévono-Dinantiens de La Méséta Marocaine: Étude Petro-Géochimique et Implication Géodynamique. Ph.D. Thesis, Bretagne Occidentale, Brest, France, 1994.
5. Aarab, E.M. Genèse et Différenciation d'un Magma Tholeïtique En Domaine Extensif Intracontinental: Exemple Du Magmatisme Pré-Orogénique Des Jbilet (Maroc Hercynien). Ph.D. Thesis, Caddi Ayyad University, Marrakech, Morocco, 1995.
6. Essaifi, A. Relations Entre Magmatisme-Déformation et Altération Hydrothermale: L'exemple Des Jebilet Centrales (Hercynien, Maroc). Ph.D. Thesis, Université Rennes, Rennes, France, 1995.
7. Ben Abbou, M. Implications Sur le Modèle Géodynamique de la Chaine Hercynienne. Master's Thesis, Université Marrakech, Marrakesh, Morocco, 2001.
8. Roddaz, M.; Bruss Et, S.; Soula, J.-C.; Béziat, D.; Abbou, M.B.; Debat, P.; Driouch, Y.; Christophoul, F.; Ntarmouchant, A.; Déramond, J. Foreland Basin Magmatism in the Western Moroccan Meseta and Geodynamic Inferences. *Tectonics* **2002**, *21*, 1, 7, 23. [CrossRef]
9. Bennouna, A.; Abbou, M.B.; Hoepffner, C.; Kharbouch, F.; Youbi, N. The Carboniferous Volcano-Sedimentary Depocentre of Tazekka Massif (Middle-Atlas, Morocco): New Observationsand Geodynamic Implications. *J. Afr. Earth Sci.* **2004**, *39*, 359–368. [CrossRef]
10. Ntarmouchant, A.; Smaili, H.; BentodosSantos, T.; Dahire, M.; Sabri, K.; Ribeiro, M.L.; Driouch, Y.; Santos, R.; Calvo, R. New Evidence of Effusive and Explosive Volcanism in theLower Carboniferous Formations of the Moroccan Central Hercynian Massif: Geochemical Dataand Geodynamic Significance. *J. Afr. Earth Sci.* **2016**, *115*, 218–233. [CrossRef]
11. Izart, A.; Tahiri, A.; El Boursoumi, A.; Chèvremont, P. Carte Géologique Du Maroc Au 1/50000, Feuille de Bouqachmir. *Notes Mémoires Serv. Géol. Maroc.* **2001**, 60.
12. Tahiri, A.; Montero, P.; El Hadi, H.; Martínez Poyatos, D.; Azor, A.; Bea, F.; Simancas, J.F.; González Lodeiro, F. Geochronological Data on the Rabat–Tiflet Granitoids: Their Bearing on the Tectonics of the Moroccan Variscides. *J. Afr. Earth Sci.* **2010**, *57*, 1–13. [CrossRef]
13. Hamoumi, N. La Plateforme Ordovicienne Du Maroc: Dynamique Des Ensembles Sedimentaires. Ph.D. Thesis, Université Louis Pasteur, Strasbourg, France, 1988.
14. Termier, H. Etudes Géologiques Sur Le Maroc Central et Le Moyen-Atlas Septentrional. Ph.D. Thesis, Imprimerie Officielle, Notes et Mémoires du Service de Géologie du Maroco; Cadi Ayyad University, Marrakesh, Morocco, 1936.
15. Piqué, A.; Michard, A. Les zones structurales du Maroc hercynien. *Sci. Géologiques Bull. Mémoires* **1981**, *34*, 135–146. [CrossRef]
16. Lazraq, N. Contribution à l'étude Micropaléontologique (Principalement Conodontes) Du Dévonien de La Région d'Oulmès (Maroc Central). Ph.D. Thesis, Sorbonne University Pierre and Marie Curie Campus, Paris, France, 1983.

17. Faik, F. Le Paleozoique de La Region de Mrirt (Est Du Maroc Central): Évolution Stratigraphique et Structurale. Ph.D. Thesis, Université Toulouse 3, Toulouse, France, 1988.
18. Bouabdelli, M. Tectonique et Sédimentation Dans Les Bassins Orogéniques: LeSillon Viséen d'Azrou-Khénifra (Est Du Massif Hercynien Central). Ph.D. Thesis, University of Strasbourg, Strasbourg, France, 1989; p. 262.
19. Habibi, M. Le Paleozoique de La Region d'ain Leuh-Souq al Had (NE Du Maroc Central): Recherches Stratigraphiques et Structurales. Master's Thesis, Université Toulouse 3, Toulouse, France, 1989; p. 186.
20. El Hassani, A. Northern Border of the Moroccan Hercynian Orogeny, Sehoul Caledonian Belt and the Northern Meseta Platform. Ph.D Thesis, Universite Louis Pasteur, Strasbourg, France, 1990.
21. Tahiri, A. Le Maroc central septentrional: Stratigraphie, sédimentologie et tectonique du paléozoïque: Un exemple de passage des zones internes aux zones externes de la chaînehercynienne du Maroc. Ph.D. Thesis, Université de Bretagne Occidentale, Brest, France, 1991.
22. Cattanéo, C.; Tahiri, A.; Vachard, D. La Sédimentation Récifale Du Givétien Dans La MesetaMarocaine Nord-Occidentale. *C. R. Acad. Des. Sci. Paris Ser.* **1993**, *317*, 73.
23. Zahraoui, M.; El Hassani, A.; Piqué, A.; Tahiri, A. LeDévonien Inférieur et Moyen. *Bull. De L'institut Sci.* **1994**, *18*, 43–56.
24. Lakhloufi, A. Etude Structurale de La Région de Brachwa, Parties Centrales et Nord-Orientale Du Bassin Dévono-Dinantien de Sidi Bettache (Maroc Nord occidental). Ph.D. Thesis, EcoleNationale Supérieure, Rabat, Morocco, 1988; 281p.
25. Ben Abbou, M.; Soula, J.-C.; Brusset, S.; Roddaz, M.; N'Tarmouchant, A.; Driouch, Y.; Christophoul, F.; Bouadbelli, M.; Majesté-Menjoulas, C.; Béziat, D.; et al. Contrôle tectonique de la sédimentation dans le système de bassins d'avant-pays de la Meseta marocaine. *C. R. De L'académie Des Sci.—Ser. IIA—Earth Planet. Sci.* **2001**, *332*, 703–709.
26. Berkhli, M.; Vachard, D. Le Carbonifère du Maroc central: Lesformations de Migoumess, deTirhela et d'Idmarrach. Lithologie, biostratigraphie et conséquences géodynamiques. *C. R. Geosci.* **2002**, *334*, 67–72. [CrossRef]
27. Hoepffner, C.; Soulaimani, A.; Piqué, A. The Moroccan Hercynides. *J. Afr. Earth Sci.* **2005**, *43*, 144–165. [CrossRef]
28. Allary, A.; Andrieux, J.; Lavenu, A.; Ribeyrolles, M. Présence de Décrochements Dans La Meseta Sud-Orientale Du Maroc Central. *C. R. De L'académie Des. Sci.* **1972**, *274*, 653–656.
29. Ben Abbou, M. Evolution Stratigraphique et Structurale, Au Cours Du Paléozoïque, de La Bordure Nord Du Massif Central (Région d'Agourai, Maroc). Master's Thesis, University of Fez, Fès, Morocco, 1990; 214p.
30. Piqué, A. *Géologie du Maroc: Les Domaines Régionaux et Leur évolution Structurale*; Imprimerie el Maarif al Jadida: Rabat, Morocco, 1994.
31. Sonnet, P. Les Skams à Tungstène, Étain et Bore de La Région d'El Hammam (Maroc Central). Ph.D. Thesis, Université Catholique de Louvain, Louvain-la-Neuve, Belgium, 1981.
32. Jébrak, M. *Contribution àl'histoire Naturelle Des Filons (F, Ba) Du Domaine Varisque. Essaide Caractérisation Structurale et Géochimique Des Filons En Extension et En Décrochement Dans Les Massifs Centraux Français et Marocain*; BRGM: Orléans, France, 1985; 473p.
33. Ntarmouchant, A. Le Magmatisme Associé à l'orogenèse Du Maroc Varisque: Exemple DuMagmatisme Du Bassin Méridional d'Azrou-Khénifra (Est Du Maroc Hercynien Central). Master's Thesis, University of Fes, Fes, Morroco, 2003.
34. Cailleux, Y. Les Écailles Anté viséennes d'Ezzeliga. Leur ImportanceDans l'interprétation Structurale Du Maroc Central. *C. R. Acad. Sci. Sér. 2 Méc. Phys. Chim. Sci. Univ. Sci. Terre* **1985**, *301*, 497–502.
35. El Wartiti, M. Le Permien Du Maroc Mesetien: Étude Géologique et Implications Paléogéographiques. Ph.D. Thesis, Université Mohammed V, Rabat, Morocco, 1990; 500p.
36. Remmal, T.; Barbarin, B.; Chairaibi, I.; El Hatimi, N. Les Granitoïdes Du District d'EI Hammam (Massif Hercynien Marocain). Mise EnPlace, Typologie et Relation Avec La Magmatogenèse Acide Tardi-Hercynienne. *Les Cah. De La Rech. I* **1999**, *1*, 77–93.
37. Saidi, A. Etat de Contrainte et Mécanismes d'ouverture et de Fermeture Des Bassins Permiens de La Meseta Marocaine. Apport de La Télédétection à La Reconnaissance Des Faciès et Des Réseaux deFailles. Ph.D. Thesis, Université Mohammed V, Rabat, Morocco, 2005.
38. Saidi, A.; Tahiri, A.; AitBrahim, L.; Saidi, M. États de contraintes et mécanismes d'ouverture et de fermeture des bassins permiens du Maroc hercynien. L'exemple des bassins des Jebilet et des Réhamna. *C. R. Geosci.* **2002**, *334*, 221–226. [CrossRef]
39. Zouine, M. Evolution Structurale Tardi-Hercynienne de La Bordure Septentrionale Du Maroc Central Entre Tiddas et Jbel Triona. Ph.D. Thesis, Ecole Nationale Supérieure, Rabat, Morocco, 1986.
40. Cogney, G.; Faugeres, J.-C. Précisions Sur La Mise EnPlace Des Épanchements BasaltiquesDes FormationsTriasiquesde La Bordure Septentrionale Du Maroc Central. *Bull. De La Société Géologique De Fr.* **1975**, *7*, 721–733. [CrossRef]
41. Et-Touhami, M.A. Le Trias Évaporitique Du Bassin de Khemisset, Maroc Central: GéométrieDes Dépôts, Évolution Sédimentaire et Géochimie. Ph.D Thesis, Claude Bernard, Lyon, France, 1992; 242p.
42. Mahmoudi, A.; Bertrand, H. Identification géochimique de la province magmatiquede l'Atlantique central en domaine plissé: Exemple du Moyen Atlas marocain. *C. R. Geosci.* **2007**, *339*, 545–552. [CrossRef]
43. Huon, S.; Piqué, A.; Clauer, N. Etude de l'orogenèse Hercynienne Au Maroc Par La Datation K-Arde l'évolution Métamorphique de Schistes Ardoisiers. *Study of the Hercynian Orogeny in Morocco by the K-Ar Isotopic Datation of Metamorphic Evolution in Slates. Sci. Géologiques Bull. Mémoires* **1987**, *40*, 273–284.
44. Tahiri, A.; Hoepffner, C. La Faille d'Oulmès: Cisaillement Ductile et TectoniqueTangentielle, Maroc Central Hercynien. *Bull. De L'institut Sci.* **1987**, *11*, 59–68.

45. Oubbih, J. Le Maroc Central Méridional (Région de Moulay Bou Azza): Stratigraphie Du Paléozoïque et Tectonique Hercynienne. Ph.D. Thesis, Univ. MedV, Rabat, Morocco, 1991.

46. Agard, J. Données Nouvelles Sur Le District Fluorifère d'El Hammam Berkamène (MarocCentral). *Rapp. Inédit SEGM* **1966**, 843.

47. Dahmani, A. Le Métamorphisme Dans l'auréole Du Granite d'Oulmès (Maroc Central): Étude pétrographique et Relation Avec Les Déformations Hercyniennes. Ph.D.Thesis, Université Mohammed V, Rabat, Morocco, 1985; 150p.

48. Diot, H. Mise En Place Des Granitoïdes Hercyniens de La Meseta Marocaine, Étude Structurale Des Massifs de Sebt de Brikine (Rehamna), de Zaër etd'Oulmès (Massif Central) et d'Aouli-Boumia (Haute Moulouya). Implications Géodynamiques. Ph.D. Thesis, UniversitéPaul Sabatier Toulouse, Toulouse, France, 1989.

49. Gasquet, D.; Stussi, J.-M.; Nachit, H. Les Granitoïdes Hercyniens Du Maroc Dans Le Cadrede l'évolution Géodynamique Régionale. *Bull. De La Société Géologique De Fr.* **1996**, *167*, 517–528.

50. Giuliani, G.; Cheilletz, A.; Zimmermann, J.L. The Emplacement, Geochemistry and Petrogenesis of Two Central Morocco Hercynian Granites.Geotectonic Implications. *J. Afr. Earth Sci. Middle East* **1989**, *9*, 617–629. [CrossRef]

51. Lagarde, J.-L. Cisaillements Ductiles et Plutons Granitiques Contemporains de La Déformation HercyniennePost Viséenne de La Méséta Marocaine. *Bull. De La Société Géologique Et Minéralogique De Bretagne* **1985**, *1*, 29–37.

52. Boushaba, A.; Cailleux, Y. Les Relations Métamorphisme-Déformation AuVoisinage Des Granitoïdes Hercyniens Du Maroc Central. *Bull. Inst.* **1992**, *16*, 15–22.

53. Mrini, Z.; Rafi, A.; Duthou, J.-L.; Vidal, P. Chronologie Rb-Sr DesGranitoidesHercyniensDuMaroc; Consequences. *Bull. De La Société Géologique De Fr.* **1992**, *163*, 281–291.

54. Amenzou, M.; El Mouraouah, A.E. Typologie Du Zircon Des Granitoïdes Hercyniens de LaMeseta Marocaine: Zonation Magmatique et Implication Géodynamique. *J. Afr. Earth Sci.* **1997**, *24*, 125–139. [CrossRef]

55. Zouhir, M. Etude Géologique Du Secteur NNE Achemmmach (Ticht Ougas): Essai d'interprétation Des Anomalies MAG (MAG Au Sol). Unpublished work.

56. Mezougane, H.; Mohamed, A.; Azizi, M.; Muhammad, S.; Mohamed, S. Analyse et Interprétation Des Données Magnétiques Au Sol Du Secteur NNE d'Achemmach (Maroc Central). *ESJ* **2019**, *15*, 139–463.

57. Cox, K.; Bell, J.; Pankhurst, R. The Interpretation of Data for Plutonic Rocks. In *The Interpretation of Igneous Rocks*; Springer: Berlin/Heidelberg, Germany, 1979; pp. 308–331.

58. Winchester, J.A.; Floyd, P.A. Geochemical Discrimination of Different Magma Series and Their Differentiation Products Using Immobile Elements. *Chem. Geol.* **1977**, *20*, 325–343. [CrossRef]

59. Pearce, J. Sources and Settings of Granitic Rocks. *Episodes* **1996**, *19*, 120–125. [CrossRef]

60. Cann, J.R. Rb, Sr, Y, Zr and Nb in Some Ocean Floor Basaltic Rocks. *Earth Planet. Sci. Lett.* **1970**, *10*, 7–11. [CrossRef]

61. Middlemost, E.A. Naming Materials in the Magma/Igneous Rock System. *Earth Sci. Rev.* **1994**, *37*, 215–224. [CrossRef]

62. De La Roche, H.; Leterrier, J.; Grandclaude, P.; Marchal, M. A Classification of Volcanic and Plutonic Rocks Using R1R2-Diagramand Major-Element Analyses—Its Relationships with Current Nomenclature. *Chem. Geol.* **1980**, *29*, 183–210. [CrossRef]

63. Shand, S.J. *Classic A/CNK vs A/NK Plot for Discriminating Metaluminous, Peraluminous and Peralkaline Compositions*; Hafner Publishing Co.: New York, NY, USA, 1943.

64. Pearce, J.A. Role of the Sub-Continental Lithosphere in Magma Genesis at Active Continental Margins. In *Continental Basalts and Mantle Xenoliths*; Hawkesworth, C.J., Norry, M.J., Eds.; Shiva Publications: Nantwich, UK, 1983; pp. 230–249.

65. Boynton, W.V. Cosmochemistry of the Rare Earth Elements: Meteorite Studies. In *Developments in Geochemistry*; Elsevier: Amsterdam, The Netherlands, 1984; Volume 2, pp. 63–114. ISBN 0921-3198.

66. Sun, S.-S.; Mc Donough, W.F. Chemical and Isotopic Systematics of Oceanic Basalts: Implicationsfor Mantle Composition and Processes. *Geol. Soc. Lond. Spec. Publ.* **1989**, *42*, 313–345. [CrossRef]

67. Driouch, Y.; Béziat, D.; Grégoire, M.; Laguenini, F.; Abbou, M.B.; Ntarmouchant, A.; Roddaz, M.; Dahire, M.; Bennouna, A.; Belkasmi, M.; et al. Clinopyroxene Trace Element Compositions of Cumulate Mafic Rocks and Basalts from the Hercynian Moroccan Central Meseta: Petrogenetic Implications. *J. Afr. Earth Sci.* **2010**, *56*, 97–106. [CrossRef]

68. Remmal, T. L'évolutionTectono-Magmatique Intracontinentale Du Cycle Hercynien. ÉtudeDu Complexe Magmatique Du District d'ElHammam et de Zones Comparables Pour Le Magmatisme Pré-Orogénique Dans LeMassif Central et Les Rehamna (Meseta Occidentale Marocaine). Ph.D. Thesis, Université de Casablanca, Casablanca, Morocco, 2000.

69. Bamoumen, H.; Aarab, E.M.; Soulaimani, A. Tectono-Sedimentary and magmatic evolution of the Upper Visean basins of Azrou-Khénifra and eastern Jebilet (Moroccan Meseta). *Estud. Geológicos* **2008**, *64*, 107–122. [CrossRef]

70. Pearce, J.A.; Norry, M.J. Petrogenetic Implications of Ti, Zr, Y, and Nb Variations in Volcanic Rocks. *Contrib. Mineral. Petrol.* **1979**, *69*, 33–47. [CrossRef]

71. Pearce, J.A. Trace Element Characteristics of Lavas from Destructive Plate Boundaries. *Andesites* **1982**, *8*, 525–548.

72. Meschede, M. A Method of Discriminating between Different Types of Mid-Ocean Ridge Basalts and Continental Tholeiites with the Nb 1b Zr 1b Y Diagram. *Chem. Geol.* **1986**, *56*, 207–218. [CrossRef]

73. Aissa, M. Etude Des Interactions Fluides-Minéraux Des Skarns à Sn, W, B d'El Hammam (Maroc Central). Facteurs Physico-Chimiques Contrôlant Le Développement Du Stade Stannifère. Ph. D. Thesis, University of Moulay Ismail, Meknes, Morocco, 1997.

74. Cabanis, B.; Lecolle, M. Le Diagramme La/10Y/15Nb/8: Un Outil Pour La Discrimination Des Sries Volcaniques et La Mise En Vidence Des Procsses de Mlange et/Ou de Contamination Crus-Tale. *CR Acad. Sci. Ser. II* **1989**, *2*, 2023–2029.